Second-order quadrupole effects on Hahn echoes in fast-rotating solids at the magic angle

Pascal P. Man
Laboratoire de Chimie des Surfaces, CNRS URA 1428, Université Pierre et Marie Curie, 4 Place Jussieu, Tour 55, 75252 Paris Cedex 05, France
(Received 5 August 1996)

In solid-state NMR, knowledge of the quadrupole coupling constant and the asymmetry parameter from a powder spectrum allows the determination of the true chemical shift of a line, which can be correlated with the mean bond angle. However, broad powder patterns are distorted by the dead time of the receiver. The common way to recover the lost signals is to apply a Hahn echo sequence. As the quadrupole interaction is a single-spin multiple-energy level interaction, the effects of multiple-quantum (MQ) transitions during the Hahn echo sequence are still not well understood. We apply the density-operator approach, combined with the order of coherence description, to predicting the echo locations of half-integer quadrupole spins ($I=\frac{3}{2}$, $\frac{5}{2}$, $\frac{7}{2}$, and $\frac{9}{2}$) in a single crystal, the amplitudes of the echoes, and the excitation conditions for obtaining quantitative results on the spin population ratio. For these purposes, the expression of the MQ transition frequency or line shift is derived. Between the two pulses and during the detection period, the rotation of the crystal at the magic angle dramatically reduces the homonuclear magnetic-dipole interaction and completely removes anisotropic spectral broadening due to the heteronuclear magnetic-dipole and the first-order quadrupole interactions; the spin system is submitted to the true isotropic chemical shift and the second-order quadrupole interactions only during these two periods. We treat in a unified way the Hahn echoes [including those involved in MQ-magic-angle spinning methodology] of the central transition representing the refocusing of single-quantum and MQ on-resonance coherences generated by the first pulse. During the pulses the crystal is assumed to be static and only the first-order quadrupole inteaction is considered; the echo amplitudes representing the refocusing of MQ coherences do not provide us with quantitative results on the spin population ratio. Only that associated with the refocusing of $1Q$ coherence gives quantitative results when the two pulse durations are short. Application to powders requires high-speed computer averaging of the echo amplitude versus one of the two pulse durations to extract the quadrupole parameters. [S0163-1829(97)00714-5]

I. INTRODUCTION

Quadrupole nuclei with a half-integer spin larger than $\frac{1}{2}$ ($I=\frac{3}{2}$, $\frac{5}{2}$, $\frac{7}{2}$, and $\frac{9}{2}$) possess a quadrupole moment Q, which interacts with the electric-field gradient (EFG) generated by their surroundings.[1–4] The coupling of Q (a property of the nucleus) with an EFG (a property of the sample) is called the quadrupole interaction H_Q. The present paper deals with the case where H_Q behaves as a weak perturbation of the Zeeman interaction $H_z=-\omega_0 I_z$ with $\omega_0=\gamma\mathbf{B}_0$, the coupling between the nuclear spin I and the external strong static magnetic field $\mathbf{B}_0$. As a result, only the first two perturbation terms of H_Q are considered: (i) the first-order quadrupole interaction $H_Q^{(1)}$, which is independent of $\mathbf{B}_0$, and (ii) the second-order quadrupole interaction $H_Q^{(2)}$, which is inversely proportional to $\mathbf{B}_0$. Quadrupole nuclei are extensively used to probe static and dynamic microscopic phenomena accompanying reversible phase transitions in solids.[5,6]

The NMR line shape of a quadrupole nucleus depends on the sample (single crystal or powder) and the strength of H_Q. The spectrum of a crystal consists of a central line, whose position is not affected by $H_Q^{(1)}$ and $2I-1$ satellite lines, whose splittings depend on $H_Q^{(1)}$. These lines are all shifted by $H_Q^{(2)}$. In most cases, the sample is a powder and its powder pattern provides us, via line-shape analysis, two parameters—the quadrupole coupling constant e^2qQ/h and the asymmetry parameter η. These two parameters allow us to determine the true isotropic chemical shift δ_{CS} of a line, which is related to the mean bond angle in a compound.[7,8] Sometimes spectra obtained with several magnetic fields $\mathbf{B}_0$ are required for the line-shape analysis. The powder pattern of all the lines will be observed if $H_Q^{(1)}$ is the dominant interaction with a small e^2qQ/h value. For example, $e^2qQ/h=118$ kHz for ^{27}Al ($I=\frac{5}{2}$) in $AlCl_3\times 6H_2O$; the central line is a symmetrical narrow line superimposed on the symmetrical broad powder pattern of the satellite lines.[9] For stronger e^2qQ/h values, the satellite-line powder pattern is difficult to detect. But rotating the sample at the magic angle θ_m with a high spinning rate makes possible the detection of spinning sidebands of satellite lines, whose envelope is nearly identical to the powder pattern of a static sample.[10] When $H_Q^{(2)}$ becomes large, the powder pattern of the central line is mainly observed, that of the satellite lines being smeared out over a MHz range. Broad powder patterns are distorted by the dead time of the receiver of a spectrometer. The common way to overcome this problem is to apply a Hahn echo sequence to recover the powder pattern of the central line[9,11,12] or that of all the lines if e^2qQ/h is not too large.[13] However, the setup of experimental conditions (durations, amplitudes, and phases of the two pulses, receiver phase, interpulse delay, and location of echoes) to excite the spin system becomes acute. Missetting one of these parameters can prevent the observation of echoes. For instance, when the interpulse delay is shorter than the duration of the free-induction decay (FID) following the second pulse, the echoes are masked by this FID. In contrast, when the inter-

pulse delay becomes much longer, the echo amplitudes are considerably reduced by spin-spin relaxation phenomena.

As H_Q is a single-spin multiple-energy level interaction, multiple-quantum (MQ) transitions between two nonconsecutive energy levels as well as single-quantum (SQ) transitions occur simultaneously during the radio-frequency (rf) pulses. Fortunately, the shift of the energy levels from those of the Zeeman interaction is only affected by the internal spin Hamiltonian H of the sample. In other words, the transitions between the energy levels of the spin system are controlled by both the pulse and H. On the other hand, the spin system evolves under H solely between the pulses and during the detection period. Therefore, the presence or the absence of pulses has a different effect on the evolution of the spin system. In the absence of pulses, one is dealing with transition frequencies between energy levels related to line positions, line shifts, and line shapes in the frequency domain. The frequency-domain studies are dominated by static[11,14–18] or mechanical rotation of the sample, namely, magic-angle spinning (MAS),[19–24] variable-angle spinning (VAS),[25–27] dynamic-angle spinning (DAS),[28–32] or double rotation (DOR).[30–33] In the presence of pulses, one is dealing with signal intensities, locations, and amplitudes of echoes in the time domain. Both aspects are present when the spin dynamics throughout the Hahn echo sequence are described by the density operator ρ.[34–36] When the latter is expressed as a matrix in the eigenstates of I_z [see Eq. (56)], the matrix elements $\rho_{r,c}$ are referred to by two half-integer magnetic numbers r and c for row and column. The elements $\rho_{r,r}$ of the main diagonal are polarizations, those of the other diagonal $\rho_{r,-r}$ are on-resonance coherences, and the remaining elements are off-resonance coherences. An element $\rho_{r,c}$ is also called an $(r-c)Q$ coherence. The MQ transition effects during the Hahn echo sequence are still not well understood.

The fact that the quadrupole interaction can be much larger than the amplitude ω_{rf} of the pulses has several implications, namely, the spin dynamics during the pulses cannot be described by a vector model of the magnetization in the rotating frame Σ^{obs} of the rf magnetic field $\mathbf{B}_1(=\omega_{\mathrm{rf}}/\gamma)$. Explicit calculation of the density operator taking into account $H_Q^{(1)}$ during the pulses is required. For example, the one-pulse experiment generates SQ as well as MQ transitions, but an rf coil can only detect $\pm 1Q$ coherences, which carry the same information. By convention the $-1Q$ coherences have been chosen. As a result, the one-pulse experiment cannot monitor the effects of MQ transitions: When the phase of the pulse is shifted by ϵ, an $(r-c)Q$ coherence undergoes an apparent phase change of $(r-c)\varepsilon$, except for the polarizations, which remain unchanged.[37–40] Analytical expressions of $(r-c)Q$ coherences for $I=\frac{3}{2}$ (Refs. 41–45), $\frac{5}{2}$ (Refs. 46 and 47), and $\frac{7}{2}$ (Refs. 48 and 49) are available; those for $I=\frac{9}{2}$ require numerical calculations.

In the case of a spin $I=\frac{1}{2}$ system, when the excitation of the spin system occurs after the spin system has reached thermodynamic equilibrium, it is well established that the relative intensity (integrated area of an absorption line) ratio of two lines in a spectrum is directly related to the relative proportion of the two site populations of the sample, whatever the pulse duration. We mean that the line intensity ratio quantitatively describes the spin population ratio. For half-integer quadrupole spins, consideration of $H_Q^{(1)}$ during the pulse in the one-pulse experiment also points out the importance of pulse duration on line intensity. The first maximum of the central-line intensity as well as the associated pulse duration decrease, but both reach limiting values when the strength of $H_Q^{(1)}$ increases.[50,51] The $\pi/2$- and π-pulse durations are not related except in two extreme cases where $H_Q^{(1)}$ is either much stronger or much smaller than ω_{rf}.[52–56] Furthermore, only a short pulse duration generates a central-line powder pattern, in agreement with that predicted by the transition-frequency calculations. Moreover, the line intensity is *proportional* to the number of spins and *independent* of the quadrupole coupling ω_Q.[21,53,55] As a result, the line intensity ratio is a quantitative measurement of the spin population ratio if the pulse duration is short. Longer pulse durations change the line intensities, and thus the spin population ratio; in the worse case they also distort the line shape.[52,53]

As the one-pulse experiment cannot monitor the MQ transition effects, a two-pulse sequence such as spin-lock,[40,45,57–59] rotary-echo,[47,60,61] two pulses with a short interpulse delay,[44,61–64] Solomon echo[65–70] or Hahn echo[9,13,71] sequences at least is required to detect the occurrence of MQ transitions during the first pulse. The second pulse converts polarizations and coherences generated by the first pulse to $-1Q$ coherences detectable by an rf coil. The conversion function has been derived for Solomon echoes[66,70] and Hahn echoes[71] for static crystals. The general approach to determining this function for a particular sequence remains to be discovered.

The present paper deals with the Hahn echoes of half-integer quadrupole spins, more particularly their locations in the detection period, and the excitation conditions for obtaining quantitative results on the spin population ratio. We choose to investigate the response of a single crystal. Application to polycrystalline samples requires high-speed computer averaging of the crystal response over all of its possible orientations.[64] In fact, the interactions considered between the two pulses and during the detection period determine the echo locations. For example, when the secular part of the heteronuclear magnetic-dipole interaction $\mathbf{\Phi} I_z$, whose expression is similar to that of the inhomogeneity of $\mathbf{B}_0$ as in the original paper of Hahn,[72] is considered during these two periods, $H_Q^{(1)}$ being present throughout the experiment, the two interactions $H_Q^{(1)}$ and ΦI_z between the two pulses dephase all the coherences generated by the first pulse. Then they refocus these coherences, via the second pulse, as echoes of the central and satellite transitions in the detection period. These echoes are located at odd numbers of the interpulse delay, which is about the duration T_{FID} of the free-induction decay of the central transition. Only the central-transition echo, representing the refocusing of the $1Q$ central-transition coherence generated by the first pulse, provides us with quantitative results on the spin population ratio if both pulse durations are short.[71] However, the homonuclear magnetic-dipole interaction $H_{D(I-I)}$—a many identical spin interaction—should be much smaller than ΦI_z, since its effects on the echoes are not well known. Up to now, the magnetic field $\mathbf{B}_0$ is not strong enough to allow us to give up the investigation of the effects of $H_Q^{(2)}$ on Hahn echoes. Only some papers deal with this problem.[73] Mainly the central-transition echo was investigated[74] and in the

selective-excitation condition.[75]

Recently, Frydman *et al.*[76,77] applied the concept of MQ spectroscopy to half-integer quadrupole spins submitted to $H_Q^{(1)}$, $H_Q^{(2)}$, and the true isotropic chemical shift Hamiltonian H_{CS} and rotating at θ_m (MQ-MAS). They showed that a two-dimensional (2D) high-resolution SQ-MQ correlation spectrum which is as good as that provided by the DAS method can be obtained. Furthermore, the two chemical shifts of a peak along the two axes of the 2D spectrum allow us to calculate the values of e^2qQ/h and η unambiguously. Rotating the sample at θ_m with a high spinning rate reduces $H_{D(I\text{-}I)}$ considerably and cancels the anisotropic broadening effects produced by ΦI_z and $H_Q^{(1)}$, which makes possible the investigation of the effects of $H_Q^{(2)}+H_{CS}$. The MQ-MAS approach[77–79] also applies a two-pulse sequence but with a complex phase cycling depending on the selected MQ coherences. Phase cycling the first pulse and the receiver allows us to select one particular pair of $\pm(r-c)Q$ coherences, which are converted to $-1Q$ coherences by the second pulse. The central-transition echoes, representing the refocusing of the $-3Q$ coherence in a spin $I=\frac{3}{2}$ system or the $-5Q$ coherence in a spin $I=\frac{5}{2}$ system, are located at unusual positions in the detection period. As long as the spinning rate of the rotor exceeds the central-transition linewidth of the static sample, synchronization of acquisition with sample rotation is not required. Indeed, none of the authors applying the two-pulse MQ-MAS approach, which regularly increments the delay between the two pulses to generate a series of files, has mentioned this experimental condition.[78–81] However, this point remains to be checked experimentally. Of course, in one-dimensional (1D) NMR, it is harmless if this synchronization is realized, which ensures that the echo is completely refocused and no additional rotational artifacts are introduced.[82]

We treat in a unified way the central-transition Hahn echoes representing the refocusing of on-resonance (SQ or MQ) coherences $\rho_{r,-r}$, generated by the first pulse. The paper is organized as follows: In Sec. II A, the expression of H_Q for a free nucleus in the absence of $\mathbf{B}_0$ is derived using the spherical tensor notation, which allows us to describe H_Q from one coordinate frame to another using the Wigner rotation matrices. In Sec. II B, the expressions of $H_Q^{(1)}$ and $H_Q^{(2)}$ of a nucleus in the presence of $\mathbf{B}_0$ are derived using the Magnus expansion. Then the second-rank spherical tensors are expressed as fourth-rank ones using the Clebsch-Gordan or Wigner coefficients. These expressions are used in Sec. II C to derive the MQ transition frequencies in the laboratory frame or the MQ line shifts relative to ω_0 for a static crystal and a crystal rotating at an arbitrary angle with respect to $\mathbf{B}_0$. For this purpose, the reduced Wigner rotation matrix of rank four is established. In Sec. II D are performed time-domain calculations. The crystal is assumed to rotate at θ_m with a high spinning rate. As the anisotropic broadening influenced by the first-order quadrupole interaction is suppressed by this rotation, only $H_Q^{(2)}$ and H_{CS} are considered between the two pulses and during the detection period. The density-operator approach, combined with the order of coherence description, is used to predict the echo locations of a spin $I=\frac{3}{2}$ system. For the spins $I=\frac{5}{2}$, $\frac{7}{2}$, and $\frac{9}{2}$, the echo locations including those involved in the MQ-MAS methodology are given. On the other hand, a numerical procedure for calculating the conversion functions or the echo amplitudes in the approximation of a static crystal during the pulses is proposed. For simplicity, only $H_Q^{(1)}$ is considered during the pulses. The results show that only the echo amplitudes representing the refocusing of the $1Q$ on-resonance coherence $\rho_{1/2,-1/2}$ generated by the first pulse provide us with quantitative results on the spin population ratio.

II. THEORY

A. Hamiltonian of the quadrupole interaction for a free nucleus in a uniform space

For simplicity, the Hamiltonians are expressed in angular frequency units. Consider a free nucleus in a uniform space, that is, the three coordinate axes x, y, and z are equivalent. The Hamiltonian representing the quadrupole interaction H_Q of this nucleus, independent of the Cartesian coordinate frame Σ, is defined by[1,2,4]

$$\hbar H_Q=\frac{eQ}{6I(2I-1)}\sum_{\kappa,\xi=x,y,z}V_{\kappa\xi}\left[\tfrac{3}{2}(I_\kappa I_\xi+I_\xi I_\kappa)-\delta_{\kappa\xi}I(I+1)\right], \tag{1}$$

with $V_{\kappa\xi}=(\partial^2U/\partial\kappa\partial\xi)_{r=0}$. $\delta_{\kappa\xi}$ is the Kronecker delta symbol, U is the electrostatic potential at the origin (inside the nucleus) generated by external charges, and $V_{\kappa\xi}$ are the Cartesian components of the EFG at the origin $\mathbf{V}$ which is a second-rank symmetrical tensor. In the principal axis system Σ^{PAS} of the EFG, $\mathbf{V}$ is diagonal,

$$\mathbf{V}=\begin{pmatrix}V_{XX}&0&0\\0&V_{YY}&0\\0&0&V_{ZZ}\end{pmatrix}, \tag{2}$$

with the convention: $|V_{ZZ}|\geqslant|V_{YY}|\geqslant|V_{XX}|$. Furthermore, the Laplace equation $V_{XX}+V_{YY}+V_{ZZ}=0$ holds for $\mathbf{V}$, because the electric field at the nucleus is produced by charges wholly external to the nucleus. Thus, only two independent parameters are required,

$$eq=V_{ZZ}, \tag{3}$$

$$\eta=\frac{V_{XX}-V_{YY}}{V_{ZZ}}, \tag{4}$$

the largest component and the asymmetry parameter, respectively, with $1\geqslant\eta\geqslant0$.

In the coordinate frame Σ^{PAS}, the Cartesian tensor representation of the quadrupole interaction [Eq. (1)] takes the form[2]

$$\hbar H_Q=\frac{e^2qQ}{4I(2I-1)}\left[3I_Z^2-I(I+1)+\eta(I_X^2-I_Y^2)\right]. \tag{5}$$

In term of the operators

$$I_+=I_X+iI_Y,\quad I_-=I_X-iI_Y, \tag{6}$$

Eq. (5) becomes[1]

$$\hbar H_Q=\frac{e^2qQ}{4I(2I-1)}\left[3I_Z^2-I(I+1)+\tfrac{1}{2}\eta(I_+^2+I_-^2)\right]. \tag{7}$$

The passage from one coordinate frame to another is more conveniently realized if the quadrupole interaction of a free nucleus is expressed as a second-rank irreducible spherical tensor:[3,83]

$$H_Q = N_Q \sum_{u=-2}^{2} (-1)^u V_{2,-u} K^{(2,u)}, \tag{8a}$$

$$N_Q = \frac{eQ}{2I(2I-1)\hbar}. \tag{8b}$$

In any Cartesian coordinate frame Σ, the spherical tensor and Cartesian tensor components of $\mathbf{V}$ are related by[3,39,83,84]

$$V_{2,0} = \tfrac{1}{2}\sqrt{6}V_{zz}, \quad V_{2,1} = -V_{xz} - iV_{yz}, \quad V_{2,-1} = V_{xz} - iV_{yz},$$

$$V_{2,2} = \tfrac{1}{2}(V_{xx} - V_{yy}) + iV_{xy}, \quad V_{2,-2} = \frac{1}{2}(V_{xx} - V_{yy}) - iV_{xy}, \tag{9}$$

and those of $\mathbf{K}$ as[83,85–87]

$$K^{(2,0)} = \tfrac{1}{6}\sqrt{6}[3I_z^2 - I(I+1)],$$

$$K^{(2,1)} = -\tfrac{1}{2}(I_z I_+ + I_+ I_z) = -\tfrac{1}{2}I_+(2I_z+1),$$

$$K^{(2,-1)} = \tfrac{1}{2}(I_z I_- + I_- I_z) = \tfrac{1}{2}I_-(2I_z-1),$$

$$K^{(2,2)} = \tfrac{1}{2}I_+ I_+, \quad K^{(2,-2)} = \tfrac{1}{2}I_- I_-, \tag{10}$$

with $I_+ = I_x + iI_y$ and $I_- = I_x - iI_y$. These two operators are different from those of Eq. (6) despite the same notation. It is worth noting that the numerical factors in the components of $\mathbf{V}$ and $\mathbf{K}$ [Eqs. (9) and (10)] depend on the authors. Using Eqs. (8)–(10), the spherical tensor representation of the quadrupole interaction in the coordinate frame Σ becomes

$$H_Q = N_Q\{\tfrac{1}{6}\sqrt{6}[3I_z^2 - I(I+1)]V_{2,0} + \tfrac{1}{2}(I_z I_+ + I_+ I_z)V_{2,-1} - \tfrac{1}{2}(I_z I_- + I_- I_z)V_{2,1} + \tfrac{1}{2}I_+^2 V_{2,-2} + \tfrac{1}{2}I_-^2 V_{2,2}\}. \tag{11}$$

Expressing Eq. (11) in Σ^{PAS} and comparing the result with Eq. (7) yield the spherical tensor components of $\mathbf{V}$ in Σ^{PAS},

$$V_{2,0}^{\mathrm{PAS}} = \tfrac{1}{2}\sqrt{6}eq, \quad V_{2,\pm1}^{\mathrm{PAS}} = 0, \quad V_{2,\pm2}^{\mathrm{PAS}} = \tfrac{1}{2}eq\,\eta. \tag{12}$$

Sometimes, the opposite convention for η is taken[14,27,28,88,89]

$$\eta = \frac{V_{YY} - V_{XX}}{V_{ZZ}}, \tag{13}$$

associated with the condition $|V_{ZZ}| \geqslant |V_{XX}| \geqslant |V_{YY}|$. As a result, a negative sign appears in front of η in Eqs. (5) and (7) and in subsequent expressions containing η. In particular, the spherical tensor components of $\mathbf{V}$ in Σ^{PAS} are[24,88,90]

$$V_{2,0}^{\mathrm{PAS}} = \tfrac{1}{2}\sqrt{6}eq, \quad V_{2,\pm1}^{\mathrm{PAS}} = 0, \quad V_{2,\pm2}^{\mathrm{PAS}} = -\tfrac{1}{2}eq\,\eta. \tag{14}$$

In the remainder of the paper, we use the first definition of η, Eq. (4).

B. Hamiltonian of the quadrupole interaction for a nucleus in a strong static magnetic field $\mathbf{B_0}$

The present paper deals with the case where H_Q can be treated as a weak perturbation of the Zeeman interaction. It is then more convenient to express interactions in the frame Σ^{obs} rotating relative to the laboratory frame Σ^{lab} with the angular frequency ω_0. Thus the spherical tensor representation of H_Q expressed by Eq. (8a) becomes time dependent[3,31,53]

$$H_Q(t) = \exp(iH_z t) H_Q \exp(-iH_z t) = N_Q \sum_{u=-2}^{2} (-1)^u V_{2,-u} K^{(2,u)} \exp(-iu\omega_0 t). \tag{15}$$

As the oscillations generated by the terms $\exp(-iu\omega_0 t)$ are very fast, we can consider only the averaged value $\langle H_Q(t)\rangle$ of $H_Q(t)$ over one Larmor period $t_L = 2\pi/\omega_0$ up to first order, using the Magnus expansion[19,53]

$$H_{Q0} = \frac{1}{t_L}\int_0^{t_L} H_Q(t)dt = N_Q V_{2,0} K^{(2,0)}, \tag{16}$$

$$H_{Q1} = -\frac{i}{2t_L}\int_0^{t_L} dt \int_0^t dt' [H_Q(t), H_Q(t')] = -\frac{N_Q^2}{\omega_0}\sum_{u\neq 0}\frac{1}{u}\{\tfrac{1}{2}V_{2,u}V_{2,-u}[K^{(2,u)}, K^{(2,-u)}] + (-1)^u V_{2,0}V_{2,-u}[K^{(2,0)}, K^{(2,u)}]\}. \tag{17}$$

This averaging makes the quadrupole interaction $H_Q(t)$ time independent: $\langle H_Q(t)\rangle = H_{Q0} + H_{Q1}$. Equation (17) differs slightly with that of Sun *et al.*[31] Developing the commutators of operators in Eq. (17) yields[19]

$$H_{Q1} = -\frac{N_Q^2}{\omega_0}\{\tfrac{1}{4}\sqrt{6}V_{2,0}V_{2,-1}I_+(2I_z+1)^2 - \tfrac{1}{4}\sqrt{6}V_{2,0}V_{2,1}I_-(2I_z-1)^2 + \tfrac{1}{2}\sqrt{6}V_{2,0}V_{2,-2}I_+^2 \times (I_z+1) + \tfrac{1}{2}\sqrt{6}V_{2,0}V_{2,2}I_-^2(I_z-1) + \tfrac{1}{2}V_{2,-1}V_{2,1}I_z \times [4I(I+1) - 8I_z^2 - 1] + \tfrac{1}{2}V_{2,-2}V_{2,2}I_z \times [2I(I+1) - 2I_z^2 - 1]\}. \tag{18}$$

Usually, only the terms of H_{Q1} that commute with I_z are considered. With this simplification, H_{Q0} and H_{Q1} are equivalent to the first-order $H_Q^{(1)}$ and the second-order terms $H_Q^{(2)}$ in the standard perturbation theory, respectively,[19,25,27]

$$H_Q^{(1)} = H_{Q0} = N_Q \tfrac{1}{6}\sqrt{6}[3I_z^2 - I(I+1)]V_{2,0}, \tag{19}$$

$$H_Q^{(2)} = H_{Q1} = -\frac{N_Q^2}{\omega_0}\{\tfrac{1}{2}V_{2,-1}V_{2,1}[4I(I+1) - 8I_z^2 - 1] + \tfrac{1}{2}V_{2,-2}V_{2,2}[2I(I+1) - 2I_z^2 - 1]\}I_z. \tag{20}$$

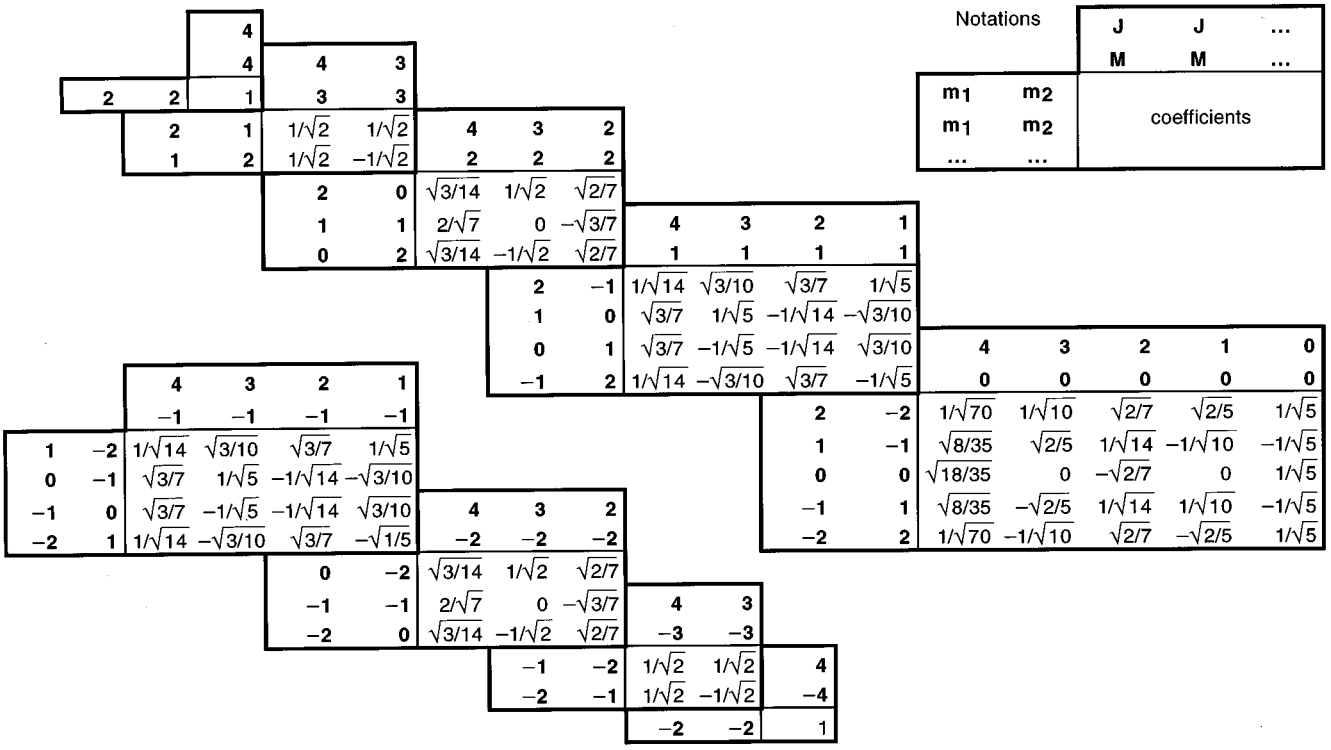

FIG. 1. $j_1=j_2=2$, Clebsch-Gordan (Ref. 92) or Wigner coefficients $\langle j_1 j_2 m_1 m_2|JM\rangle$, which can be calculated with the MATHEMATICA function Clebsch Gordan [{j_1,m_1}, {j_2,m_2}, {J, M}]. Reading down one column in the table gives the coefficients in the expansion $W_{J,M}=\Sigma_{m_1 m_2}\langle j_1 j_2 m_1 m_2|JM\rangle V_{j_1,m_1}V_{j_2,m_2}$, and reading across one row gives the coefficients in $V_{j_1,m_1}V_{j_2,m_2}=\Sigma_{J,M}\langle j_1 j_2 m_1 m_2|JM\rangle W_{J,M}$. In fact nine tables are shown.

Equations (19) and (20), derived in the rotating frame $\Sigma^{\rm obs}$, are unchanged in the laboratory frame $\Sigma^{\rm lab}$. This is because they commute with the Zeeman interaction. From now on, we shall use the language of standard perturbation theory. The first-order quadrupole interaction $H_Q^{(1)}$ is independent of ω_0 and is an even function of I_z. In contrast, the second-order quadrupole interaction $H_Q^{(2)}$ is inversely proportional to ω_0 and is an odd function of I_z as the heteronuclear magnetic-dipole interaction ΦI_z. Therefore, a strong static magnetic field is required to reduce the effects of $H_Q^{(2)}$. Equation (20) can be rewritten with commutators of operators as[32,91]

$$H_Q^{(2)}=-\frac{N_Q^2}{\omega_0}\{V_{2,1}V_{2,-1}[K^{(2,1)},K^{(2,-1)}] + \tfrac{1}{2}V_{2,2}V_{2,-2}[K^{(2,2)},K^{(2,-2)}]\}. \quad (21)$$

The two sets of direct products of the spin (**K**) and the EFG (**V**) second-rank irreducible tensors appearing in Eq. (21) can be expressed as the spin (**L**) and the EFG (**W**) spherical tensors of higher rank, respectively, using the Clebsch-Gordan or Wigner coefficients[92] reported in Fig. 1 (Refs. 33 and 93),

$$H_Q^{(2)}=-\frac{N_Q^2}{\omega_0}\{\tfrac{1}{70}\sqrt{7}W_{4,0}(17L^{(3,0)}-6L^{(1,0)}) + \tfrac{1}{35}\sqrt{35}W_{2,0}(3L^{(3,0)}+L^{(1,0)}) - \tfrac{1}{10}\sqrt{2}W_{0,0}(3L^{(3,0)}-4L^{(1,0)})\}. \quad (22)$$

These coefficients can also be calculated with the MATHEMATICA function Clebsch Gordan [{j_1,m_1}, {j_2,m_2},{J,M}]. To obtain the expressions of $L^{(1,0)}$ and $L^{(3,0)}$, we express once more the two products $V_{2,-1}V_{2,1}$ and $V_{2,-2}V_{2,2}$ of $H_Q^{(2)}$ in Eq. (20), as linear combinations of the EFG (**W**) spherical tensor components, using the Clebsch-Gordan or Wigner coefficients. Then comparing the new expression of $H_Q^{(2)}$ with that of Eq. (22) allows us to deduce that[33]

$$L^{(1,0)}=\tfrac{1}{5}\sqrt{10}[I(I+1)-\tfrac{3}{4}]I_z, \quad (23a)$$

$$L^{(3,0)}=\tfrac{1}{5}\sqrt{10}[3I(I+1)-5I_z^2-1]I_z. \quad (23b)$$

However, the two tensor operators $L^{(1,0)}$ and $L^{(3,0)}$ are unnormalized. When we express them with normalized tensor operators $P^{(1,0)}$ and $P^{(3,0)}$ defined by[85,86]

$$L^{(1,0)}=\tfrac{1}{5}\sqrt{10}[I(I+1)-\tfrac{3}{4}]P^{(1,0)}, \quad (24a)$$

$$L^{(3,0)}=-2P^{(3,0)}, \quad (24b)$$

Eq. (22) is rewritten as

$$H_Q^{(2)}=-\frac{N_Q^2}{\omega_0}\left\{-\frac{17}{5\sqrt{7}}W_{4,0}P^{(3,0)}-\tfrac{3}{35}\sqrt{\frac{14}{5}}[I(I+1)-\tfrac{3}{4}]\right.$$
$$\times W_{4,0}P^{(1,0)}-\frac{6}{\sqrt{35}}W_{2,0}P^{(3,0)}+\frac{\sqrt{14}}{35}[I(I+1)-\tfrac{3}{4}]$$
$$\times W_{2,0}P^{(1,0)}+\frac{3\sqrt{2}}{5}W_{0,0}P^{(3,0)}$$
$$\left.+\frac{4}{5\sqrt{5}}[I(I+1)-\tfrac{3}{4}]W_{0,0}P^{(1,0)}\right\}. \quad (25)$$

Equations (20), (22), and (25) are three ways to express the second-order quadrupole interaction. In the next section the three tensor components $W_{0,0}$, $W_{2,0}$, and $W_{4,0}$ in Eqs. (22) and (25) will be related to the two quantities eq and η.

C. Multiple-quantum line shift

The $(r-c)Q$ transition frequency between two energy levels $|r\rangle$ and $|c\rangle$ in Σ^{lab} becomes an $(r-c)Q$ line shift with respect to ω_0 (angular frequency of Σ^{obs}) in the spectrum. In angular frequency unit, this $(r-c)Q$ line shift $\omega_{r,c}$ is defined by

$$\omega_{r,c}=\langle r|(H_Q^{(1)}+H_Q^{(2)})|r\rangle-\langle c|(H_Q^{(1)}+H_Q^{(2)})|c\rangle=\omega_{r,c}^{(1)}+\omega_{r,c}^{(2)}. \quad (26)$$

The $(r-c)Q$ line shift produced by the first-order quadrupole interaction or the $(r-c)Q$ first-order quadrupole shift $\omega_{r,c}^{(1)}$ is given by

$$\omega_{r,c}^{(1)}=N_Q\tfrac{1}{2}\sqrt{6}(r^2-c^2)V_{2,0}. \quad (27)$$

For symmetrical transition $(c=-r)$ this shift is null. This fact leads to the development of MQ-MAS techniques[76–82,94–97] and overtone NMR.[93,98] The $(r-c)Q$ second-order quadrupole shift $\omega_{r,c}^{(2)}$ is given by

$$\omega_{r,c}^{(2)}=-\frac{N_Q^2}{\omega_0}(r-c)\left\{\frac{1}{70}\sqrt{\frac{35}{2}}W_{4,0}A^{(4)}\right.$$
$$\left.+\frac{1}{28}\sqrt{14}W_{2,0}A^{(2)}-\frac{1}{\sqrt{5}}W_{0,0}A^{(0)}\right\}, \quad (28)$$

with

$$A^{(4)}(I,r,c)=18I(I+1)-34(r^2+rc+c^2)-5,$$
$$A^{(2)}(I,r,c)=8I(I+1)-12(r^2+rc+c^2)-3,$$
$$A^{(0)}(I,r,c)=I(I+1)-3(r^2+rc+c^2). \quad (29)$$

For symmetrical transition the relationships of Eq. (29) become identical to those of Amoureux.[94] In the remainder of the paper, an $(r-c)Q$ shift is shorten as a shift for simplicity.

1. Static single crystal

For a static single crystal, the tensor component $V_{2,0}$ in Eqs. (19) and (27) is related to those expressed in Σ^{PAS} by

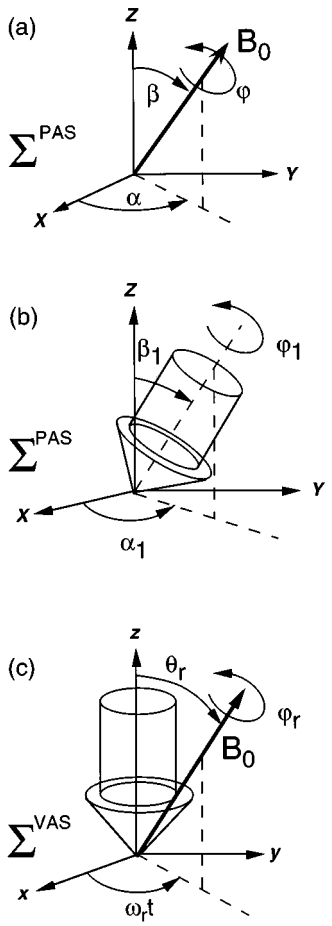

FIG. 2. Euler angles for static (a) and variable-angle spinning (b), (c) experiments. In (a) these angles orientate the strong static magnetic field $\mathbf{B}_0$ in the principal-axis-system coordinate frame Σ^{PAS} of the electric-field gradient tensor; α and β are also the polar angles of $\mathbf{B}_0$. In (b) the angles α_1, β_1, and φ_1 orientate the spinner in the coordinate frame Σ^{PAS} and in (c) the polar angles $\omega_r t$ and θ_r show the direction of $\mathbf{B}_0$ in the coordinate frame Σ^{VAS} of the spinner.

$$V_{2,0}=\sum_{u=-2}^{2}V_{2,u}^{\text{PAS}}D_{u,0}^{(2)}(\alpha,\beta,\varphi)$$
$$=\frac{1}{2}\sqrt{6}eq[\tfrac{1}{2}(3\cos^2\beta-1)+\tfrac{1}{2}\eta\sin^2\beta\cos2\alpha], \quad (30)$$

the Wigner rotation matrix $D^{(2)}(\alpha,\beta,\varphi)$ can be found in text books.[83,88,99–101] The first two Euler angles α and β are the polar angles of $\mathbf{B}_0$ in Σ^{PAS} [Fig. 2(a)]. The third Euler angle φ does not appear in Eq. (30), because $\mathbf{B}_0$ is a symmetry axis for the spins. Therefore, the first-order quadrupole interaction [Eq. (19)] becomes

$$H_Q^{(1)}=\tfrac{1}{3}\omega_Q[3I_z^2-I(I+1)], \quad (31)$$

with the quadrupole coupling ω_Q defined by

$$\omega_Q=\tfrac{3}{4}\Omega_Q[3\cos^2\beta-1+\eta\sin^2\beta\cos2\alpha], \quad (32a)$$

TABLE I. Principal-axis-system elements of the EFG spherical tensor **W** as a linear combination of products of those of the second-rank EFG spherical tensor **V**, using the Clebsch-Gordon or Wigner coefficients[92] reported in Fig. 1 (Refs. 31 and 33).

k,n	$W^{\mathrm{PAS}}_{k,n}$	
0,0	$\frac{1}{\sqrt{5}}[2(V^{\mathrm{PAS}}_{2,2})^2+(V^{\mathrm{PAS}}_{2,0})^2]$	$\frac{\sqrt{5}}{10}(eq)^2(\eta^2+3)$
2,0	$\frac{\sqrt{14}}{7}[2(V^{\mathrm{PAS}}_{2,2})^2-(V^{\mathrm{PAS}}_{2,0})^2]$	$\frac{1}{\sqrt{14}}(eq)^2(\eta^2-3)$
2,±2	$\frac{4}{\sqrt{14}}V^{\mathrm{PAS}}_{2,2}V^{\mathrm{PAS}}_{2,0}$	$\sqrt{\frac{3}{7}}(eq)^2\eta$
4,0	$\frac{2}{\sqrt{70}}[(V^{\mathrm{PAS}}_{2,2})^2+3(V^{\mathrm{PAS}}_{2,0})^2]$	$\frac{1}{\sqrt{70}}(eq)^2\left(\frac{1}{2}\eta^2+9\right)$
4,±2	$\frac{6}{\sqrt{42}}V^{\mathrm{PAS}}_{2,2}V^{\mathrm{PAS}}_{2,0}$	$\frac{3}{2\sqrt{7}}(eq)^2\eta$
4,±4	$(V^{\mathrm{PAS}}_{2,2})^2$	$\frac{1}{4}(eq)^2\eta^2$

$$\Omega_Q=eqN_Q=\frac{e^2qQ}{2I(2I-1)\hbar}. \tag{32b}$$

Sometimes, a minus sign appears in front of η in Eq. (32a) even when the first convention for η [Eq. (4)] is applied; this is due to the choice of another set of Euler angles where the two angles α and β are not the polar angles of $\mathbf{B}_0$.[99] Our quadrupole coupling ω_Q is equal to half the standard one,[1] which means that two consecutive lines in the spectrum of a single crystal are separated by $2\omega_Q$, if the second-order quadrupole interaction is zero. For polycrystalline samples, the quadrupole coupling constant e^2qQ/h and the asymmetry parameter η are the relevant quantities.

The tensor components $W_{4,0}$, $W_{2,0}$, and $W_{0,0}$ are related to those expressed in Σ^{PAS}, $W^{\mathrm{PAS}}_{k,n}$ (Table I), by the Wigner rotation matrices $D^{(2k)}(\alpha,\beta,\varphi)$ as

$$W_{2x,0}=\sum_{u=-x}^{x}W^{\mathrm{PAS}}_{2x,2u}D^{(2x)}_{2u,0}(\alpha,\beta,\varphi). \tag{33}$$

The reduced Wigner rotation matrix $d^{(4)}(\beta)$ associated with $D^{(4)}(\alpha,\beta,\varphi)$ is defined in Table II. The matrix elements can also be obtained using the MATHEMATICA program written by Zare.[86] Equation (28) becomes

$$\omega^{(2)}_{r,c}=-\frac{r-c}{2\omega_0}\Omega_Q^2\sum_{k}^{0,1,2}A^{(2k)}(I,r,c)\times\sum_{u=-k}^{k}B_{2k,2u}(\eta)D^{(2k)}_{2u,0}(\alpha,\beta,\varphi), \tag{34}$$

with[94]

$$B_{0,0}(\eta)=-\tfrac{1}{5}(\eta^2+3),\quad B_{2,0}(\eta)=\tfrac{1}{14}(\eta^2-3),$$

$$B_{2,\pm2}(\eta)=\tfrac{1}{14}\eta\sqrt{6},\quad B_{4,0}(\eta)=\tfrac{1}{140}(\eta^2+18),$$

$$B_{4,\pm2}(\eta)=\tfrac{3}{140}\eta\sqrt{10},\quad B_{4,\pm4}(\eta)=\frac{1}{4\sqrt{70}}\eta^2. \tag{35}$$

2. Rotating single crystal

For a single crystal rotating at an angle θ_r with respect to $\mathbf{B}_0$, this experimental condition corresponds to that of VAS,[25–27] the component $V_{2,0}$ in the first-order quadrupole shift [Eq. (27)] is related to those expressed in Σ^{PAS}, $V^{\mathrm{PAS}}_{2,n}$, by two Wigner rotation matrices $D^{(2)}(\alpha_1,\beta_1,\varphi_1)$ and $D^{(2)}(\omega_r t,\theta_r,\varphi_r)$ as

$$V^{\mathrm{VAS}}_{2,u}=\sum_{j=-2}^{2}V^{\mathrm{PAS}}_{2,j}D^{(2)}_{j,u}(\alpha_1,\beta_1,\varphi_1), \tag{36a}$$

$$V_{2,0}=\sum_{u=-2}^{2}V^{\mathrm{VAS}}_{2,u}D^{(2)}_{u,0}(\omega_r t,\theta_r,\varphi_r). \tag{36b}$$

The first Wigner rotation matrix $D^{(2)}(\alpha_1,\beta_1,\varphi_1)$ describes the orientation of the spinner fixed in Σ^{PAS} with the Euler angles α_1, β_1, and φ_1 [Fig. 2(b)]. The second Wigner rotation matrix $D^{(2)}(\omega_r t,\theta_r,\varphi_r)$ describes the orientation of $\mathbf{B}_0$ in the coordinate frame of the spinner Σ^{VAS}, the polar angles $\omega_r t$ and θ_r are those of $\mathbf{B}_0$ [Fig. 2(c)]. The third Euler angle φ_r will not appear explicitly for the same reason as in the case for static experiments. Equation (27) becomes

$$\omega^{(1)\mathrm{VAS}}_{r,c}=N_Q\tfrac{1}{2}\sqrt{6}(r^2-c^2)\sum_{u=-2}^{2}D^{(2)}_{u,0}(\omega_r t,\theta_r,\varphi_r)\times\sum_{j=-2}^{2}V^{\mathrm{PAS}}_{2,j}D^{(2)}_{j,u}(\alpha_1,\beta_1,\varphi_1). \tag{37}$$

Similarly the components $W_{4,0}$, $W_{2,0}$, and $W_{0,0}$ in the second-order quadrupole shift are related to those expressed in Σ^{PAS}, $W^{\mathrm{PAS}}_{k,n}$ (Table I), by two Wigner rotation matrices $D^{(2x)}(\alpha_1,\beta_1,\varphi_1)$ and $D^{(2x)}(\omega_r t,\theta_r,\varphi_r)$ as

$$W^{\mathrm{VAS}}_{2x,u}=\sum_{j=-x}^{x}W^{\mathrm{PAS}}_{2x,2j}D^{(2x)}_{2j,u}(\alpha_1,\beta_1,\varphi_1), \tag{38a}$$

$$W_{2x,0}=\sum_{u=-2x}^{2x} W_{2x,u}^{\mathrm{VAS}} D_{u,0}^{(2x)}(\omega_r t,\theta_r,\varphi_r). \tag{38b}$$

Equation (28) becomes

$$\omega_{r,c}^{(2)\mathrm{VAS}}=-\frac{r-c}{2\omega_0}\,\Omega_Q^2\sum_{x=0}^{2} A^{(2x)}(I,r,c)\sum_{u=-2x}^{2x} D_{u,0}^{(2x)} \times(\omega_r t,\theta_r,\varphi_r)\sum_{j=-x}^{x} B_{2x,2j}(\eta)D_{2j,u}^{(2x)}(\alpha_1,\beta_1,\varphi_1). \tag{39}$$

The terms $\exp(-iu\omega_r t)$ of $D_{u,0}^{(2x)}(\omega_r t,\theta_r,\varphi_r)$ in Eq. (39) give rise to spinning sidebands in the frequency domain. The amplitude of nth sideband depends on $1/(n\omega_r)$,[102] and is thus suppressed at high spinning rate. Under the *high spinning* condition, that is, upon ignoring oscillating terms such as $\exp(-iu\omega_r t)$ due to the rotation of the spinner, only the elements $D_{0,0}^{(2x)}(\omega_r t,\theta_r,\varphi_r)$ of the Wigner rotation matrices $D^{(2x)}$ remain nonzero, that is, the elements with the subscript $u=0$ in Eqs. (37) and (39). As a result, the two angles $\omega_r t$ and φ_1 will not appear explicitly in the expressions of the line shift. The first- and second-order quadrupole shifts become

$$\omega_{r,c}^{(1)\text{fast VAS}}=N_Q\tfrac{1}{2}\sqrt{6}(r^2-c^2)d_{0,0}^{(2)}(\theta_r)\sum_{j=-2}^{2} V_{2,j}^{\mathrm{PAS}} D_{j,0}^{(2)} \times(\alpha_1,\beta_1,\varphi_1), \tag{40a}$$

$$\begin{aligned}\omega_{r,c}^{(2)\text{fast VAS}}&=-\frac{r-c}{2\omega_0}\,\Omega_Q^2\sum_{x=0}^{2} A^{(2x)}(I,r,c)d_{0,0}^{(2x)} \times(\theta_r)\sum_{j=-x}^{x} B_{2x,2j}(\eta)D_{2j,0}^{(2x)}(\alpha_1,\beta_1,\varphi_1)\\ &=-\frac{r-c}{2\omega_0}\,\Omega_Q^2\{A^{(0)}(I,r,c)B_{0,0}(\eta)\\ &\quad+A^{(2)}(I,r,c)d_{0,0}^{(2)}(\theta_r)[B_{2,0}(\eta)d_{0,0}^{(2)}(\beta_1)\\ &\quad+2B_{2,2}(\eta)d_{2,0}^{(2)}(\beta_1)\cos 2\alpha_1]+A^{(4)}(I,r,c)d_{0,0}^{(4)}\\ &\quad\times(\theta_r)[B_{4,0}(\eta)d_{0,0}^{(4)}(\beta_1)+2B_{4,2}(\eta)d_{2,0}^{(4)}\\ &\quad\times(\beta_1)\cos 2\alpha_1+2B_{4,4}(\eta)d_{4,0}^{(4)}(\beta_1)\cos 4\alpha_1]\}.\end{aligned} \tag{40b}$$

The three reduced Wigner rotation matrix elements $d_{0,0}^{(0)}(\theta_r)$, $d_{0,0}^{(2)}(\theta_r)$, and $d_{0,0}^{(4)}(\theta_r)$ are identical to the three Legendre polynomials $P_0(\cos\theta_r)$, $P_2(\cos\theta_r)$, and $P_4(\cos\theta_r)$, respectively:[27,28,33,100,103]

$$P_0(\cos\theta_r)=1, \tag{41a}$$

$$P_2(\cos\theta_r)=\tfrac{1}{2}(3\cos^2\theta_r-1), \tag{41b}$$

$$P_4(\cos\theta_r)=\tfrac{1}{8}(35\cos^4\theta_r-30\cos^2\theta_r+3). \tag{41c}$$

For symmetrical transition Eq. (40a) reduces to zero as in static experiment, Eq. (40b) becomes identical to that of Amoureux[94] or Frydman and Harwood:[76]

$$\begin{aligned}\omega_{r,-r}^{(2)\text{fast VAS}}&=-\frac{\Omega_Q^2}{\omega_0}\{2r[I(I+1)-3r^2][\tfrac{1}{2}B_{0,0}(\eta)]\\ &\quad+2r[8I(I+1)-12r^2-3](\tfrac{1}{2})[B_{2,0}(\eta)d_{0,0}^{(2)}\\ &\quad\times(\beta_1)+2B_{2,2}(\eta)d_{2,0}^{(2)}(\beta_1)\cos 2\alpha_1]\\ &\quad\times P_2(\cos\theta_r)+2r[18I(I+1)-34r^2-5](\tfrac{1}{2})\\ &\quad\times[B_{4,0}(\eta)d_{0,0}^{(4)}(\beta_1)+2B_{4,2}(\eta)d_{2,0}^{(4)}\\ &\quad\times(\beta_1)\cos 2\alpha_1+2B_{4,4}(\eta)d_{4,0}^{(4)}\\ &\quad\times(\beta_1)\cos 4\alpha_1]P_4(\cos\theta_r)\}.\end{aligned} \tag{42}$$

For the central transition ($r=-\frac{1}{2}$) Eq. (42) becomes

$$\begin{aligned}\omega_{-1/2,1,2}^{(2)\text{fast VAS}}&=\frac{\Omega_Q^2}{\omega_0}[I(I+1)-\tfrac{3}{4}]\{\tfrac{1}{2}B_{0,0}(\eta)+8(\tfrac{1}{2})\\ &\quad\times[B_{2,0}(\eta)d_{0,0}^{(2)}(\beta_1)+2B_{2,2}(\eta)d_{2,0}^{(2)}\\ &\quad\times(\beta_1)\cos 2\alpha_1]P_2(\cos\theta_r)+18(\tfrac{1}{2})\\ &\quad\times[B_{4,0}(\eta)d_{0,0}^{(4)}(\beta_1)+2B_{4,2}(\eta)d_{2,0}^{(4)}\\ &\quad\times(\beta_1)\cos 2\alpha_1+2B_{4,4}(\eta)d_{4,0}^{(4)}\\ &\quad\times(\beta_1)\cos 4\alpha_1]P_4(\cos\theta_r)\},\end{aligned} \tag{43}$$

with

$$\begin{aligned}&\tfrac{1}{2}\,B_{0,0}(\eta)=-\tfrac{3}{10}\,(\tfrac{1}{3}\,\eta^2+1),\quad 4B_{2,0}(\eta)=\tfrac{6}{7}\,(\tfrac{1}{3}\,\eta^2-1),\\ &4B_{2,\pm 2}(\eta)=\frac{12}{7\sqrt{6}}\,\eta,\quad 9B_{4,0}(\eta)=\frac{81}{70}\left(\frac{1}{18}\,\eta^2+1\right),\\ &9B_{4,\pm 2}(\eta)=\frac{27}{14\sqrt{10}}\,\eta,\quad 9B_{4,\pm 4}(\eta)=\frac{9}{4\sqrt{70}}\,\eta^2.\end{aligned} \tag{44}$$

Equations (43) and (44) are similar to those of Zheng *et al.*,[27] except they applied the second convention for η [Eq. (13)]. Compared with those of Llor and Virlet,[28] who also used the second convention for η, the relationships of Eq. (44) must be divided by 9, because they used the coefficient $9\Omega_Q^2$ instead of Ω_Q^2 in Eq. (43).

3. Second-order quadrupole shift of the center of gravity of a spectrum

For a powder sample, the absorption line of the central transition $(-\frac{1}{2},\frac{1}{2})$ in the presence of the second-order quadrupole interaction has a characteristic normalized shape $f(\omega)$ depending on the experiments (static, VAS or MAS in the limit of high spinning rate) and a center of gravity $\omega_{-1/2,1/2}^{(2)\mathrm{iso}}$ independent of the experiments (static, VAS, DAS, DOR, or MAS). From the definition of the first moment M_1 with respect to a frequency ω_a given, in the rotating frame Σ^{obs}, by

$$M_1=\int_{-\infty}^{\infty}(\omega-\omega_a)f(\omega)d\omega,$$

TABLE II. Reduced rotation matrix elements $d^{(4)}_{m,n}(\beta)$ of the fourth-rank Wigner rotation matrix $D^{(4)}(\alpha,\beta,\varphi)$, whose elements are defined by $D^{(4)}_{m,n}(\alpha,\beta,\varphi)=\exp(-im\alpha)d^{(4)}_{m,n}(\beta)\exp(-in\varphi)$. For simplicity, $c\equiv\cos\beta$ and $s\equiv\sin\beta$. These reduced matrix elements are related by the symmetry relationships $d^{(k)}_{m,n}(\beta)=(-1)^{m-n}d^{(k)}_{n,m}(\beta)$, $d^{(k)}_{m,n}(\beta)=(-1)^{m-n}d^{(k)}_{-m,-n}(\beta)$, and $d^{(k)}_{m,n}(\beta)=(-1)^{k-n}d^{(k)}_{m,-n}(\beta+\pi)$, (Refs. 27, 86, and 100).

m \ n	4	3	2	1	0	−1	−2	−3	−4
4	$\frac{1}{16}(1+c)^4$	$-\frac{\sqrt{2}}{8}(1+c)^3 s$	$\frac{\sqrt{7}}{8}(1+c)^2 s^2$	$-\frac{\sqrt{14}}{8}(1+c)s^3$	$\frac{\sqrt{70}}{16}s^4$	$-\frac{\sqrt{14}}{8}(1-c)s^3$	$\frac{\sqrt{7}}{8}(1-c)^2 s^2$	$-\frac{\sqrt{2}}{8}(1-c)^3 s$	$\frac{1}{16}(1-c)^4$
3	$\frac{\sqrt{2}}{8}(1+c)^3 s$	$-\frac{1}{8}(1+c)^3$ $\times(3-4c)$	$\frac{\sqrt{14}}{8}(1+c)^2$ $\times(1-2c)s$	$-\frac{\sqrt{7}}{8}(1+c)$ $\times(1-4c)s^2$	$-\frac{\sqrt{35}}{4}cs^3$	$\frac{\sqrt{7}}{8}(1-c)$ $\times(1+4c)s^2$	$-\frac{\sqrt{14}}{8}(1-c)^2$ $\times(1+2c)s$	$\frac{1}{8}(1-c)^3$ $\times(3+4c)$	$-\frac{\sqrt{2}}{8}(1-c)^3 s$
2	$\frac{\sqrt{7}}{8}(1+c)^2 s^2$	$-\frac{\sqrt{14}}{8}(1+c)^2$ $\times(1-2c)s$	$\frac{1}{4}(1+c)^2$ $\times(7c^2-7c+1)$	$-\frac{\sqrt{2}}{8}(1+c)$ $\times(14c^2-7c-1)s$	$\frac{\sqrt{10}}{8}(7c^2-1)s^2$	$-\frac{\sqrt{2}}{8}(1-c)$ $\times(14c^2+7c-1)s$	$\frac{1}{4}(1-c)^2$ $\times(7c^2+7c+1)$	$-\frac{\sqrt{14}}{8}(1-c)^2$ $\times(1+2c)s$	$\frac{\sqrt{7}}{8}(1-c)^2 s^2$
1	$\frac{\sqrt{14}}{8}(1+c)s^3$	$-\frac{\sqrt{7}}{8}(1+c)$ $\times(1-4c)s^2$	$\frac{\sqrt{2}}{8}(1+c)(14c^2$ $-7c-1)s$	$\frac{1}{8}(1+c)(3-6c$ $-12c^2+28c^3)$	$-\frac{\sqrt{5}}{4}(7c^2-3)cs$	$-\frac{1}{8}(1-c)(3+6c$ $-21c^2-28c^3)$	$-\frac{\sqrt{2}}{8}(1-c)(14c^2$ $+7c-1)s$	$\frac{\sqrt{7}}{8}(1-c)$ $\times(1+4c)s^2$	$-\frac{\sqrt{14}}{8}(1-c)s^3$
0	$\frac{\sqrt{70}}{16}s^4$	$\frac{\sqrt{35}}{4}cs^3$	$\frac{\sqrt{10}}{8}(7c^2-1)s^2$	$\frac{\sqrt{5}}{4}(7c^2-3)cs$	$\frac{1}{8}(35c^4-30c^2+3)$	$-\frac{\sqrt{5}}{4}(7c^2-3)cs$	$\frac{\sqrt{10}}{8}(7c^2-1)s^2$	$-\frac{\sqrt{35}}{4}cs^3$	$\frac{\sqrt{70}}{16}s^4$
−1	$\frac{\sqrt{14}}{8}(1-c)s^3$	$\frac{\sqrt{7}}{8}(1-c)$ $\times(1+4c)s^2$	$\frac{\sqrt{2}}{8}(1-c)(14c^2$ $+7c-1)s$	$-\frac{1}{8}(1-c)(3+6c$ $-21c^2-28c^3)$	$\frac{\sqrt{5}}{4}(7c^2-3)cs$	$\frac{1}{8}(1+c)(3-6c$ $-21c^2+28c^3)$	$-\frac{\sqrt{2}}{8}(1+c)$ $\times(14c^2-7c-1)s$	$-\frac{\sqrt{7}}{8}(1+c)$ $\times(1-4c)s^2$	$-\frac{\sqrt{14}}{8}(1+c)s^3$
−2	$\frac{\sqrt{7}}{8}(1-c)^2 s^2$	$\frac{\sqrt{14}}{8}(1-c)^2$ $\times(1+2c)s$	$\frac{1}{4}(1-c)^2$ $\times(7c^2+7c+1)$	$\frac{\sqrt{2}}{8}(1-c)(14c^2$ $+7c-1)s$	$\frac{\sqrt{10}}{8}(7c^2-1)s^2$	$\frac{\sqrt{2}}{8}(1+c)(14c^2$ $-7c-1)s$	$\frac{1}{4}(1+c)^2$ $\times(7c^2-7c+1)$	$\frac{\sqrt{14}}{8}(1+c)^2$ $\times(1-2c)s$	$\frac{\sqrt{7}}{8}(1+c)^2 s^2$
−3	$\frac{\sqrt{2}}{8}(1-c)^3 s$	$\frac{1}{8}(1-c)^3$ $\times(3+4c)$	$\frac{\sqrt{14}}{8}(1-c)^2$ $\times(1+2c)s$	$\frac{\sqrt{7}}{8}(1-c)$ $\times(1+4c)s^2$	$\frac{\sqrt{35}}{4}cs^3$	$-\frac{\sqrt{7}}{8}(1+c)$ $\times(1-4c)s^2$	$-\frac{\sqrt{14}}{8}(1+c)^2$ $\times(1-2c)s$	$-\frac{1}{8}(1+c)^3$ $\times(3-4c)$	$-\frac{\sqrt{2}}{8}(1+c)^3 s$
−4	$\frac{1}{16}(1-c)^4$	$\frac{\sqrt{2}}{8}(1-c)^3 s$	$\frac{\sqrt{7}}{8}(1-c)^2 s^2$	$\frac{\sqrt{14}}{8}(1-c)s^3$	$\frac{\sqrt{70}}{16}s^4$	$\frac{\sqrt{14}}{8}(1+c)s^3$	$\frac{\sqrt{7}}{8}(1+c)^2 s^2$	$\frac{\sqrt{2}}{8}(1+c)^3 s$	$\frac{1}{16}(1+c)^4$

with

$$\int_{-\infty}^{\infty} f(\omega)d\omega = 1, \tag{45a}$$

M_1 becomes zero when ω_a is the center of gravity $\omega^{(2)\text{iso}}_{-1/2,1/2}$. The latter is not located at the Larmor frequency. For this reason, this deviation is called the second-order quadrupole shift of the center of gravity $\omega^{(2)\ \text{iso}}_{r,c}$ of a spectrum:

$$\omega^{(2)\text{iso}}_{-1/2,1/2} = \int_{-\infty}^{\infty} \omega^{(2)}_{-1/2,1/2} f(\omega)d\omega. \tag{45b}$$

Equation (45b) means that $\omega^{(2)\text{iso}}_{-1/2,1/2}$ is the average value of the line position $\omega^{(2)}_{-1/2,1/2}$. In this paragaph, we extend the definition of center of gravity to any transition (r,c). Of course, in 1D NMR only $\omega^{(2)\text{iso}}_{-1/2,1/2}$ is observed. On the other hand, $\omega^{(2)\text{iso}}_{r,c}$ is extensively used in 2D MQ-MAS spectra. Theoretically, $\omega^{(2)\text{iso}}_{r,c}$ is defined by the same relationship independent of the kind of experiments, that is, by integrating over all possible crystallite orientations of the second-order quadrupole shift $\omega^{(2)}_{r,c}$ with equal probability $1/(4\pi)$:

$$\begin{aligned}\omega^{(2)\text{iso}}_{r,c} &= \frac{1}{4\pi}\int_{-1}^{1} d(\cos\beta)\int_{0}^{2\pi}\omega^{(2)}_{r,c}d\alpha \\ &= -\frac{r-c}{2\omega_0}\,\Omega_Q^2 A^{(0)}(I,r,c)B_{0,0}(\eta) \\ &= \frac{r-c}{2\omega_0}\,\Omega_Q^2[I(I+1)-3(r^2+rc+c^2)] \\ &\quad\times(\tfrac{3}{5})(1+\tfrac{1}{3}\eta^2),\end{aligned} \tag{45c}$$

where we used the expression of $\omega^{(2)\text{fast VAS}}_{r,c}$ defined in Eq. (40b). For symmetrical transition Eq. (45c) simplifies to

$$\omega^{(2)\text{iso}}_{r,-r} = \frac{r}{\omega_0}\,\Omega_Q^2[I(I+1)-3r^2](\tfrac{3}{5})(1+\tfrac{1}{3}\eta^2). \tag{46}$$

For the central transition Eq. (46) reduces to

$$\omega^{(2)\text{iso}}_{-1/2,1/2} = -\frac{3\Omega_Q^2}{10\omega_0}[I(I+1)-\tfrac{3}{4}](1+\tfrac{1}{3}\eta^2). \tag{47}$$

Our second-order quadrupole shift of the center of gravity of a spectrum and that defined by Medek, Harwood, and Frydman[77] ν_0^Q are related by $\frac{1}{3}\omega^{(2)\ \text{iso}}_{-1/2,1/2} = 2\pi\nu_0^Q$.

In MAS experiments the angle θ_r corresponds to the magic angle θ_m, the root of $P_2(\cos\theta_r)=0$. Under the high spinning condition, the first order [see Eq. (40a)] and the second-order quadrupole shifts [see Eq. (40b)] become

$$\omega^{(1)\text{fast MAS}}_{r,c} = 0, \tag{48a}$$

$$\begin{aligned}\omega^{(2)\text{fast MAS}}_{r,c} &= \omega^{(2)\text{iso}}_{r,c} - \frac{r-c}{2\omega_0}\,\Omega_Q^2 A^{(4)}(I,r,c)[B_{4,0}(\eta)d^{(4)}_{0,0}(\beta_1) \\ &\quad + 2B_{4,2}(\eta)d^{(4)}_{2,0}(\beta_1)\cos 2\alpha_1 + 2B_{4,4}(\eta)d^{(4)}_{4,0} \\ &\quad\times(\beta_1)\cos 4\alpha_1]P_4(\cos\theta_m).\end{aligned} \tag{48b}$$

The first-order quadrupole shift is reduced to zero either by the high spinning of the crystal at θ_m or by the restriction to on-resonance (or symmetrical) transitions; that of the second order is simpler. Equation (48b) is the result of frequency-domain calculation and will be extensively used in the next section to determine the locations of the central-transition Hahn echoes of a spin $I=\frac{3}{2}$ system submitted to the second-order quadrupole interaction and the true isotropic chemical shift between the two pulses and during the detection period.

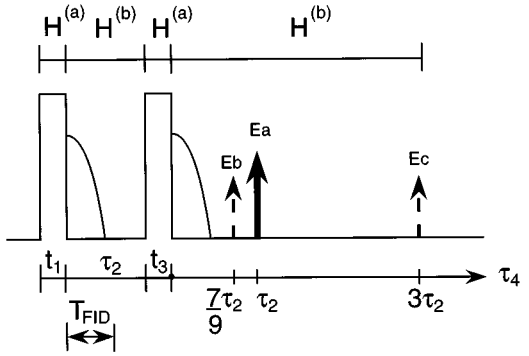

FIG. 3. Pulse sequence, Hamiltonians ($H^{(a)}=H_{\text{rf}}+H_Q^{(1)}$; $H^{(b)}=H_{\text{CS}}+H_Q^{(2)\text{fast MAS}}$), and $p=-1$ central-transition Hahn echoes for a spin $I=\frac{3}{2}$ system. Echoes are depicted schematically by arrows, whose heights and widths are meaningless. The echoes Ea, Eb, and Ec represent the refocusing of $1Q$, $-3Q$, and $\pm 3Q$ on-resonance coherences generated by the first pulse, respectively.

D. Locations and amplitudes of the spin-$\frac{3}{2}$ Hahn echoes for a single crystal rotating at magic angle with high spinning rate

The Hahn echo sequence is shown in Fig. 3. Our aim is to determine the locations and the amplitudes of the spin-$\frac{3}{2}$ central-transition echoes in the detection period. In practice, these echoes are the only ones detected when the sample is a powder. For instance, the product $(e^2qQ/h)\sqrt{1+\frac{1}{3}\eta^2}$ is about 2 MHz for the three crystallographic sites of ^{87}Rb ($I=\frac{3}{2}$) in $RbNO_3$, only the central transition echoes were observed with a 7 T magnetic field.[29,78,80] Once the matrix element $\rho^{E}_{-1/2,1/2}(t_1,\tau_2,t_3,\tau_4)$ of the echo density operator is determined, the x and y component of the *relative* echo amplitudes are defined by[9,13]

$$\begin{aligned}&E_x(t_1,\tau_2,t_3,\tau_4) + iE_y(t_1,\tau_2,t_3,\tau_4) \\ &\quad = \frac{\sqrt{I(I+1)+(1/4)}}{\frac{1}{3}\ I(I+1)(2I+1)}\,\rho^{E}_{-1/2,1/2}(t_1,\tau_2,t_3,\tau_4).\end{aligned} \tag{49}$$

In the remainder of the paper, we consider a spin $I=\frac{3}{2}$ system in a crystal rotating at θ_m with a high spinning rate. Therefore, homonuclear magnetic-dipole interaction is considerably reduced. Spectral broadening effects due to heteronuclear magnetic-dipole interaction and chemical shift anisotropy are averaged out as well. Moreover, only on-resonance coherences $\rho_{r,-r}$ developed at the end of the first pulse are considered, because their transition frequencies are equal to that of Σ^{obs}.[104] Throughout the paper, the matrices associated with Hamiltonians and density operators are expressed in the eigenstates $|r\rangle$ of I_z. A matrix element is referred to with subscripts: two half-integer magnetic num-

bers r and c associated with a row and a column of a matrix [see Eq. (56)]. The order p of an $(r-c)Q$ coherence $\rho_{r,c}$ is defined by $p=r-c$. A pulse may cause coherences to be transferred from one order to another whereas free precession preserves the coherence order[37,105,106]

This section consists of three parts: In Sec. III D 1, to follow the evolution of the spin system throughout the experiment, we employ the density-operator approach and the coherence-order description. The interactions during the two pulses do not need to be defined explicitly for the moment. During the interpulse delay τ_2 and the detection period τ_4, the Hamiltonian $H^{(b)}$ of the spin system, expressed in the rotating frame Σ^{obs} of the central transition, consists of two terms:

$$H^{(b)}=H_{\text{CS}}+H_Q^{(2)\text{fast MAS}}, \tag{50a}$$

with $H_{\text{CS}}=-\delta_{\text{CS}}\omega_0 I_z$, because the contribution of the first-order quadrupole interaction to the line shift is canceled by the high spinning of the crystal. The analytical expression of $H_Q^{(2)\text{fast MAS}}$ is unknown but it is defined by the corresponding line shift or second-order quadrupole shift [Eq. (48b)],

$$\omega_{r,c}^{(2)\text{fast MAS}}=\langle r|H_Q^{(2)\text{fast MAS}}|r\rangle-\langle c|H_Q^{(2)\text{fast MAS}}|c\rangle. \tag{50b}$$

In Sec. III D 2, we derive the central-transition Hahn echo locations as well as the associated echo amplitudes, whose maximum is modulated by a phase factor. One of these echoes is involved in the MQ-MAS methodology.

In Sec. III D 3, a numerical procedure for calculating the conversion functions or the echo amplitudes is proposed and illustrated for the spin $I=\frac{3}{2}$ system. For simplicity the two pulse durations t_1 and t_3 must be much shorter than the inverse of the spinner angular velocity, so that during the pulses the spinner looks static. In other words, the interactions are time independent during the pulses.[77] Under these assumptions, the Hamiltonian $H^{(a)}$ of the spin system consists of four terms during the pulses,

$$H^{(a)}=H_{\text{rf}}+H_{\text{CS}}+H_Q^{(1)\text{static}}+H_Q^{(2)\text{static}}. \tag{51a}$$

$H_Q^{(1)\text{static}}$ is defined by Eq. (31) and $H_Q^{(2)\text{static}}$ by Eqs. (20), (22), or (25). If Eq. (20) is used for $H_Q^{(2)\text{static}}$, the following expressions are required:[99]

$$\begin{aligned}V_1V_{-1}=&-\tfrac{3}{4}e^2q^2\{[-\tfrac{1}{3}(\eta\cos2\alpha)^2+2\eta\cos2\alpha-3]\cos^4\beta\\&+[\tfrac{2}{3}(\eta\cos2\alpha)^2-2\eta\cos2\alpha-\tfrac{1}{3}\eta^2+3]\cos^2\beta\\&+\tfrac{1}{3}\eta^2(1-\cos^2 2\alpha)\},\end{aligned}$$

$$\begin{aligned}V_2V_{-2}=&\tfrac{3}{2}e^2q^2\{[\tfrac{1}{24}(\eta\cos2\alpha)^2-\tfrac{1}{4}\eta\cos2\alpha+\tfrac{3}{8}]\cos^4\beta\\&+[-\tfrac{1}{12}(\eta\cos2\alpha)^2+\tfrac{1}{6}\eta^2-\tfrac{3}{4}]\cos^2\beta\\&+\tfrac{1}{24}(\eta\cos2\alpha)^2+\tfrac{1}{4}\eta\cos2\alpha+\tfrac{3}{8}\}.\end{aligned} \tag{51b}$$

As a first approach, we neglect $H_Q^{(2)\text{static}}$ and H_{CS} during the pulses and consider the remaining two terms,

$$H^{(a)}=H_{\text{rf}}+H_Q^{(1)\text{static}}, \tag{51c}$$

when experiments are performed at high magnetic field $\mathbf{B}_0$.[77] Two $-x$ pulses are considered. These assumptions are identical to those of our previous study on a Hahn echo sequence applied to static crystals.[71]

1. Description of the evolution of the spin system using density operators

For a spin $I=\frac{3}{2}$ system submitted to the interactions defined in Eq. (50a), the line shifts $\omega_{p/2,-p/2}^{\text{fast MAS}}$ associated with the coherence order $p=3(\frac{3}{2}\leftrightarrow-\frac{3}{2})$, 1 $(\frac{1}{2}\leftrightarrow-\frac{1}{2})$, -1 $(-\frac{1}{2}\leftrightarrow\frac{1}{2})$, and -3 $(-\frac{3}{2}\leftrightarrow\frac{3}{2})$ are

$$\omega_{3/2,-3/2}^{\text{fast MAS}}=3\omega_{-1/2,1/2}^{(2)\text{iso}}+\tfrac{7}{9}\xi_{-1/2,1/2}-3\delta_{\text{CS}}\omega_0, \tag{52a}$$

$$\omega_{1/2,-1/2}^{\text{fast MAS}}=-\omega_{-1/2,1/2}^{(2)\text{iso}}-\xi_{-1/2,1/2}-\delta_{\text{CS}}\omega_0, \tag{52b}$$

$$\omega_{-1/2,1/2}^{\text{fast MAS}}=\omega_{-1/2,1/2}^{(2)\text{iso}}+\xi_{-1/2,1/2}+\delta_{\text{CS}}\omega_0, \tag{52c}$$

$$\omega_{-3/2,3/2}^{\text{fast MAS}}=-3\omega_{-1/2,1/2}^{(2)\text{iso}}-\tfrac{7}{9}\xi_{-1/2,1/2}+3\delta_{\text{CS}}\omega_0, \tag{52d}$$

respectively, with

$$\begin{aligned}\xi_{r,-r}=&-\frac{\Omega_Q^2}{\omega_0}rA^{(4)}(I,r,-r)[B_{4,0}(\eta)d_{0,0}^{(4)}(\beta_1)\\&+2B_{4,2}(\eta)d_{2,0}^{(4)}(\beta_1)\cos2\alpha_1+2B_{4,4}(\eta)d_{4,0}^{(4)}\\&\times(\beta_1)\cos4\alpha_1]P_4(\cos\theta_m),\end{aligned} \tag{53a}$$

or simply

$$\omega_{p/2,-p/2}^{\text{fast MAS}}=\omega_{p/2,-p/2}^{(2)\text{fast MAS}}-p\delta_{\text{CS}}\omega_0. \tag{53b}$$

For a spin $I=\frac{3}{2}$ system, $\xi_{-1/2,1/2}\propto 27\Omega_Q^2/\omega_0$ and $\omega_{-1/2,1/2}^{(2)\text{iso}}=-9\Omega_Q^2(1+\frac{1}{3}\eta^2)/(10\omega_0)$. The line shifts for the other three half-integer quadrupole spins ($I=\frac{5}{2}$, $\frac{7}{2}$, and $\frac{9}{2}$) are reported in the Appendix.

We follow the spin dynamics from the thermodynamic equilibrium to the detection period using density operators. In the high-temperature approximation, the initial state is described by the density operator $\rho(0)=I_z$, whose coherence order is $p=0$. At the end of the first pulse the density operator is defined by[9,13]

$$\rho(t_1)=T\exp(-i\Omega t_1)T^\dagger\rho(0)T\exp(i\Omega_1)T^\dagger, \tag{54}$$

where Ω and T are the diagonalized form of $H^{(a)}$ and the transformation operator related by

$$\Omega=T^\dagger H^{(a)}T. \tag{55}$$

Equation (55) is solved numerically using standard diagonalization procedure, which is applicable for any half-integer quadrupole spin and whatever the complexity of $H^{(a)}$. For a spin $I=\frac{3}{2}$ system, the density operator $\rho(t_1)$ has the following general matrix form:

$$\rho(t_1)=\begin{array}{c} \\ \langle\frac{3}{2}| \\ \langle\frac{1}{2}| \\ \langle-\frac{1}{2}| \\ \langle-\frac{3}{2}| \end{array}\begin{array}{c} \begin{array}{cccc} |\frac{3}{2}\rangle & |\frac{1}{2}\rangle & |-\frac{1}{2}\rangle & |-\frac{3}{2}\rangle \end{array} \\ \begin{bmatrix} \langle I_z^{3/2,-3/2}(t_1)\rangle & \langle I_-^{3/2,1/2}(t_1)\rangle & \langle I_-^{3/2,-1/2}(t_1)\rangle & -i\langle I_y^{3/2,-3/2}(t_1)\rangle \\ \langle I_+^{3/2,1/2}(t_1)\rangle & \langle I_z^{1/2,-1/2}(t_1)\rangle & -i\langle I_y^{1/2,-1/2}(t_1)\rangle & \langle I_-^{1/2,-3/2}(t_1)\rangle \\ \langle I_+^{3/2,-1/2}(t_1)\rangle & i\langle I_y^{1/2,-1/2}(t_1)\rangle & -\langle I_z^{1/2,-1/2}(t_1)\rangle & \langle I_-^{-1/2,-3/2}(t_1)\rangle \\ i\langle I_y^{3/2,-3/2}(t_1)\rangle & \langle I_+^{1/2,-3/2}(t_1)\rangle & \langle I_+^{-1/2,-3/2}(t_1)\rangle & -\langle I_z^{3/2,-3/2}(t_1)\rangle \end{bmatrix} \end{array} \tag{56}$$

where $\langle I_q^{r,c}(t_1)\rangle=\mathrm{Tr}[\rho(t_1)I_q^{r,c}]$ indicates a nonequilibrium state of phase coherence between the two connected states $|r\rangle$ and $|c\rangle$. The spin operators $I_q^{r,c}$ were defined previously.[9,37] The matrix element $\langle I_-^{r,c}(t_1)\rangle$ is an $(r-c)Q$ coherence and $\langle I_+^{r,c}(t_1)\rangle$ a $-(r-c)Q$ coherence. According to MQ transition formalism,[37] the matrix of Eq. (56) can be decomposed as a sum of seven simpler matrices $\rho_p(t_1)$ defined in Table III,

$$\rho(t_1)=\sum_{p=-3}^{3}\rho_p(t_1). \tag{57}$$

The analytical expressions of the density-operator components $\rho_p(t_1)$ are unknown. They are defined only by their matrix forms. In particular $\rho_p(t_1)=\rho_{-p}^{\dagger}(t_1)$. As we restrict the study to on-resonance coherences developed at the end of the first pulse, Eq. (57) simplifies to a sum of four terms $\rho_p^S(t_1)$,

$$\rho^S(t_1)=\sum_{p}^{-3,-1,1,3}\rho_p^S(t_1), \tag{58}$$

where $\rho_p^S(t_1)$ contains only a single nonzero element $[\rho_p]_{p/2,-p/2}$ of the corresponding matrix ρ_p. The superscript s means ''simplified.'' In particular $\rho_{\pm 3}^S(t_1)=\rho_{\pm 3}(t_1)$, and

$$\rho_1^S(t_1)=\begin{bmatrix} 0 & 0 & 0 & 0 \\ 0 & 0 & -i\langle I_y^{1/2,-1/2}\rangle & 0 \\ 0 & 0 & 0 & 0 \\ 0 & 0 & 0 & 0 \end{bmatrix},\quad \rho_{-1}^S(t_1)=\begin{bmatrix} 0 & 0 & 0 & 0 \\ 0 & 0 & 0 & 0 \\ 0 & i\langle I_y^{1/2,-1/2}\rangle & 0 & 0 \\ 0 & 0 & 0 & 0 \end{bmatrix}. \tag{59}$$

At the end of the interpulse delay τ_2, the density operator becomes

$$\rho^S(t_1,\tau_2)=\exp(-iH^{(b)}\tau_2)\left[\sum_{p}^{-3,-1,1,3}\rho_p^S(t_1)\right]\exp(iH^{(b)}\tau_2)=\sum_{p}^{-3,-1,1,3}\rho_p^S(t_1)\exp(-i\tau_2\omega_{p/2,-p/2}^{\text{fast MAS}}), \tag{60a}$$

or in the matrix form,

$$\rho^S(t_1,\tau_2)=\begin{bmatrix} 0 & 0 & 0 & -i\langle I_y^{3/2,-3/2}(t_1)\rangle\times e^{-i\tau_2\omega_{3/2,-3/2}^{\text{fast MAS}}} \\ 0 & 0 & -i\langle I_y^{1/2,-1/2}(t_1)\rangle\times e^{-i\tau_2\omega_{1/2,-1/2}^{\text{fast MAS}}} & 0 \\ 0 & i\langle I_y^{1/2,-1/2}(t_1)\rangle\times e^{-i\tau_2\omega_{-1/2,1/2}^{\text{fast MAS}}} & 0 & 0 \\ i\langle I_y^{3/2,-3/2}(t_1)\rangle\times e^{-i\tau_2\omega_{-3/2,3/2}^{\text{fast MAS}}} & 0 & 0 & 0 \end{bmatrix}. \tag{60b}$$

TABLE III. Matrix representation of the density operator components $\rho_p(t_1)$ at the end of the first rf pulse for a spin $I=\frac{3}{2}$ system, t_1 is the first-pulse duration and p is the order of coherence.

$$\rho_3(t_1)=\begin{bmatrix}0&0&0&-i\langle I_y^{3/2,-3/2}\rangle\\0&0&0&0\\0&0&0&0\\0&0&0&0\end{bmatrix},\quad \rho_{-3}(t_1)=\begin{bmatrix}0&0&0&0\\0&0&0&0\\0&0&0&0\\i\langle I_y^{3/2,-3/2}\rangle&0&0&0\end{bmatrix}$$

$$\rho_2(t_1)=\begin{bmatrix}0&0&\langle I_-^{3/2,-1/2}\rangle&0\\0&0&0&\langle I_-^{1/2,-3/2}\rangle\\0&0&0&0\\0&0&0&0\end{bmatrix},\quad \rho_{-2}(t_1)=\begin{bmatrix}0&0&0&0\\0&0&0&0\\\langle I_+^{3/2,-1/2}\rangle&0&0&0\\0&\langle I_+^{1/2,-3/2}\rangle&0&0\end{bmatrix}$$

$$\rho_1(t_1)=\begin{bmatrix}0&\langle I_-^{3/2,1/2}\rangle&0&0\\0&0&-i\langle I_y^{1/2,-1/2}\rangle&0\\0&0&0&\langle I_-^{1/2,-3/2}\rangle\\0&0&0&0\end{bmatrix},\quad \rho_{-1}(t_1)=\begin{bmatrix}0&0&0&0\\\langle I_+^{3/2,1/2}\rangle&0&0&0\\0&i\langle I_y^{1/2,-1/2}\rangle&0&0\\0&0&\langle I_+^{1/2,-3/2}\rangle&0\end{bmatrix}$$

$$\rho_0(t_1)=\begin{bmatrix}\langle I_z^{3/2,-3/2}\rangle&0&0&0\\0&\langle I_z^{1/2,-1/2}\rangle&0&0\\0&0&-\langle I_z^{1/2,-1/2}\rangle&0\\0&0&0&-\langle I_z^{3/2,-3/2}\rangle\end{bmatrix}$$

The effect of the second pulse on the density operator $\rho^S(t_1,\tau_2)$ is described by

$$\rho^S(t_1,\tau_2,t_3)=T\ \exp(-i\Omega t_3)T^\dagger\rho^S(t_1,\tau_2)T\ \exp(i\Omega t_3)T^\dagger. \tag{61}$$

As a pulse affects only the spin part of a Hamiltonian, Eq. (61) can be rewritten as

$$\begin{aligned}\rho^S(t_1,\tau_2,t_3)&=T\ \exp(-i\Omega t_3)T^\dagger\Bigg[\sum_p^{-3,-1,1,3}\rho_p^S(t_1)\\&\quad\times\exp(-i\tau_2\omega_{p/2,-p/2}^{\text{fast MAS}})\Bigg]T\exp(i\Omega t_3)T^\dagger\\&=\sum_p^{-3,-1,1,3}\rho_p^S(t_1,t_3)\exp(-i\tau_2\omega_{p/2,-p/2}^{\text{fast MAS}}),\end{aligned} \tag{62}$$

with

$$\rho_p^S(t_1,t_3)=T\ \exp(-i\Omega t_3)T^\dagger\rho_p^S(t_1)T\ \ \exp(i\Omega t_3)T^\dagger. \tag{63}$$

During the detection period τ_4 the density operator becomes

$$\rho^S(t_1,\tau_3,t_3,\tau_4)=\exp(-iH^{(b)}\tau_4)\rho^S(t_1,\tau_2,t_3)\exp(iH^{(b)}\tau_4). \tag{64}$$

2. Locations of the Hahn echoes in the detection period

We are concerned with the $p=-1$ central-transition coherence in the detection period,

$$\rho^S_{-1/2,1/2}(t_1,\tau_2,t_3,\tau_4)=\rho^S_{-1/2,1/2}(t_1,\tau_3,t_3)\times\exp(-i\tau_4\omega_{-1/2,1/2}^{\text{fast MAS}}), \tag{65}$$

which is the only coherence detectable in our assumptions. The matrix element $\rho^S_{-1/2,1/2}(t_1,\tau_2,t_3)$ is that of the density operator $\rho^S(t_1,\tau_2,t_3)$ at the end of the second pulse. Using Eq. (62), Eq. (65) is rewritten as

$$\begin{aligned}\rho^S_{-1/2,1/2}(t_1,\tau_2,t_3,\tau_4)&=\exp(-i\tau_4\omega_{-1/2,1/2}^{\text{fast MAS}})\\&\quad\times\sum_p^{-3,-1,1,3}[\rho_p^S(t_1,t_3)]_{-1/2,1/2}\\&\quad\times\exp(-i\tau_2\omega_{p/2,-p/2}^{\text{fast MAS}}).\end{aligned} \tag{66}$$

The four coherence orders (-3, -1, 1, and 3) present at the end of the first pulse [Eq. (63)] contribute to the $p=-1$ central-transition coherence in the detection period.

For $p=1$, because $\omega_{-1/2,1/2}^{\text{fast MAS}}=-\omega_{1/2,-1/2}^{\text{fast MAS}}$, an echo appears at $\tau_4=\tau_2$, whose expression is

$$\rho^E_{-1/2,1/2}(t_1,\tau_2,t_3,\tau_4)=\exp[-i(\tau_4-\tau_2)\omega_{-1/2,1/2}^{\text{fast MAS}}]\times[\rho_1^S(t_1,t_3)]_{-1/2,1/2}. \tag{67}$$

This echo is represented schematically in Fig. 3 by the arrow Ea. Its maximum is independent of $\omega_{-1/2,1/2}^{\text{fast MAS}}$. Applying Eq. (63), Eq. (67) becomes

$$\rho^E_{-1/2,1/2}(t_1,\tau_2,t_3,\tau_4=\tau_2)=[\rho^S_1(t_1,t_3)]_{-1/2,1/2}$$
$$=[T\ \exp(-i\Omega t_3)T^\dagger\rho^S_1(t_1)T \times\exp(i\Omega t_3)T^\dagger]_{-1/2,1/2}. \quad (68)$$

It shows that the second pulse refocuses as an echo the coherence associated with the single nonzero matrix element of $\rho^S_1(t_1)$, the $p=1$ central-transition coherence generated by the first pulse or $[\rho^S_1(t_1)]_{1/2,-1/2}=-i\langle I_y^{1/2,-1/2}(t_1)\rangle$. It is called in the remainder of the paper $1Q$ $\tau_4=\tau_2$ echo.

The coherence order $p=-1$ does not generate an echo, because both exponential functions for $p=-1$ in Eq. (66) differ only by the durations τ_2 and τ_4:

$$\rho^E_{-1/2,1/2}(t_1,\tau_2,t_3,\tau_4)=\exp[-i(\tau_4+\tau_2)\omega^{\text{fast MAS}}_{-1/2,1/2}] \times[\rho^S_1(t_1,t_3)]_{-1/2,1/2}. \quad (69)$$

For $p=3$, an echo is predicted but it originates only from one of the three terms contained in Eq. (52a). Its expression is

$$\rho^E_{-1/2,1/2}(t_1,\tau_2,t_3,\tau_4)$$
$$=\exp[-i(\tau_4-3\tau_2)\delta_{\rm CS}\omega_0][\rho^S_3(t_1,t_3)]_{-1/2,1/2} \times\exp[-i\tau_4(\omega^{(2)\text{iso}}_{-1/2,1/2}+\xi_{-1/2,1/2})] \times\exp[-i\tau_2(3\omega^{(2)\text{iso}}_{-1/2,1/2}+\tfrac{7}{9}\xi_{-1/2,1/2})]. \quad (70)$$

This echo is located at $\tau_4=3\tau_2$ and is represented schematically in Fig. 3 by the arrow Ec. At its maximum, the echo does not depend on $H_{\rm CS}$ [last term in Eq. (52a)], but depends on the second-order quadrupole interaction terms as a phase modulation:

$$\rho^E_{-1/2,1/2}(t_1,\tau_2,t_3,\tau_4=3\tau_2)$$
$$=[\rho^S_3(t_1,t_3)]_{-1/2,1/2} \times\exp[-i\tau_2(6\omega^{(2)\text{iso}}_{-1/2,1/2}+\tfrac{34}{9}\xi_{-1/2,1/2})]. \quad (71)$$

This echo represents the refocusing of the $p=3$ coherence generated by the first pulse or $[\rho^S_3(t_1)]_{3/2,-3/2}=-i\langle I_y^{3/2,-3/2}(t_1)\rangle$. It is called $3Q$ $\tau_4=3\tau_2$ echo. We suppose the acquisition of the time-domain signal starts at the top of the echo. In two-dimensional SQ-$3Q$ correlation NMR spectroscopy where the F_2 dimension corresponds to the usual SQ axis related to τ_4 and the F_1 dimension corresponds to the MQ axis related to τ_2, the center of gravity of the spectrum along F_1 is located at $6\omega^{(2)\text{iso}}_{-1/2,1/2}$ instead of $\delta_{\rm CS}\omega_0+\omega^{(2)\text{iso}}_{-1/2,1/2}$ along F_2, and the linewidth is proportional to $\frac{34}{9}\xi_{-1/2,1/2}$ in F_1 instead of $\xi_{-1/2,1/2}$ in F_2.

For $p=-3$, two echoes are predicted. Their expressions deduced from Eq. (66) are

$$\rho^E_{-1/2,1/2}(t_1,\tau_2,t_3,\tau_4)$$
$$=[\rho^S_{-3}(t_1,t_3)]_{-1/2,1/2}\{\exp[-i(\tau_4-3\tau_2)\omega^{(2)\text{iso}}_{-1/2,1/2}] \times\exp[-i\tau_4(\xi_{-1/2,1/2}+\delta_{\rm CS}\omega_0)] \times\exp[-i\tau_2(-\tfrac{7}{9}\xi_{-1/2,1/2}+3\delta_{\rm CS}\omega_0)] +\exp[-i(\tau_4-\tfrac{7}{9}\tau_2)\xi_{-1/2,1/2}]\exp[-i\tau_4(\omega^{(2)\text{iso}}_{-1/2,1/2} +\delta_{\rm CS}\omega_0)]\exp[-i\tau_2(-3\omega^{(2)\text{iso}}_{-1/2,1/2}+3\delta_{\rm CS}\omega_0)]\}. \quad (72)$$

Both echoes represent the refocusing of the $p=-3$ coherence generated by the first pulse or $[\rho^S_{-3}(t_1)]_{-3/2,3/2}=i\langle I_y^{3/2,-3/2}(t_1)\rangle$. The first echo is located at $\tau_4=3\tau_2$ and is also represented in Fig. 3 by the arrow Ec. It is called the $-3Q$ $\tau_4=3\tau_2$ echo. In contrast to the $3Q$ $\tau_4=3\tau_2$ echo, this one does not depend on the second-order quadrupole shift of the center of gravity [first term in Eq. (52d)] but depends on the other two terms of Eq. (52d) as a phase modulation:

$$\rho^E_{-1/2,1/2}(t_1,\tau_2,t_3,\tau_4=3\tau_2)$$
$$=[\rho^S_{-3}(t_1,t_3)]_{-1/2,1/2} \times\exp[-i\tau_2(\tfrac{20}{9}\xi_{-1/2,1/2}+6\delta_{\rm CS}\omega_0)]. \quad (73)$$

In two-dimensional SQ-$3Q$ correlation spectroscopy, the spectrum located at $6\delta_{\rm CS}\omega_0$ along the F_1 dimension has a linewidth proportional to $\frac{20}{9}\xi_{-1/2,1/2}$. As the $\pm3Q$ $\tau_4=3\tau_2$ echoes cannot be observed independently, their maximum carry the same information as a free-induction decay. To observe them, the interpulse delay τ_2 must be large enough so that the $1Q$ $\tau_4=\tau_2$ echo and the $\pm3Q$ $\tau_4=3\tau_2$ echoes are separated. Equation (72) shows that another echo, located at $\tau_4=7\tau_2/9$ (Ref. 76), is predicted [second term in Eq. (52d)]. This echo is represented schematically by the arrow Eb in Fig. 3. It is called $-3Q$ $\tau_4=7\tau_2/9$ echo. At its maximum, the echo depends only on two shifts, the second-order quadrupole shift of the center of gravity of a spectrum and the chemical shift as a phase modulation:

$$\rho^E_{-1/2,1/2}(t_1,\tau_2,t_3,\tau_4=\tfrac{7}{9}\tau_2)$$
$$=[\rho^S_{-3}(t_1,t_3)]_{-1/2,1/2} \times\exp[-i\tau_2(-\tfrac{20}{9}\omega^{(2)\text{iso}}_{-1/2,1/2}+\tfrac{34}{9}\delta_{\rm CS}\omega_0)]. \quad (74)$$

This phase modulation leads to the development of MQ-MAS methodology,[76–82,94–97] which gives the same information as the DAS approach.[29] The line is located at $-\frac{20}{9}\omega^{(2)\text{iso}}_{-1/2,1/2}+\frac{34}{9}\delta_{\rm CS}\omega_0$ along F_1 without linewidth, which leads to a high-resolution spectrum along F_1. It is striking that among the four echoes predicted above, only the maximum of the usual $1Q$ $\tau_4=\tau_2$ echo is not modulated in phase.

As the spin-spin relaxation, not explicitly considered in our assumptions, drastically reduces the amplitudes of the echoes occurring far from the second pulse, it is advantageous to study the $-3Q$ $\tau_4=7\tau_2/9$ echo rather than the $\pm3Q$ $\tau_4=3\tau_2$ echoes. However, this echo is disturbed by the $1Q$ $\tau_4=\tau_2$ echo. Fortunately, six-phase cycling[77,78] of the first pulse and the receiver cancels the $1Q$ $\tau_4=\tau_2$ echo and allows the observation of the $-3Q$ $\tau_4=7\tau_2/9$ echo. This six-phase

TABLE IV. Echo locations and phase modulation $\exp(-i\tau_2\phi)$ of the maximum echo amplitude for the four half-integer quadrupole spins I and the coherence orders p. For clarity, $\omega \equiv \omega^{(2)\mathrm{iso}}_{-1/2,1/2}$ is the second-order quadrupole shift of the center of gravity of a spectrum, $\xi \equiv \xi_{-1/2,1/2}$ is related to the MQ line width, and $\delta \equiv \delta_{\mathrm{CS}}\ \omega_0$ is the true isotropic chemical shift. The first two parameters are spin-dependent. The symbol $*$ indicates the echo locations involved in MQ-MAS.

I	3/2		5/2		7/2		9/2	
p	Echo location	ϕ	Echo location	ϕ	Echo location	ϕ	Echo location	ϕ
$9Q$							$\tau_4=9\tau_2$	$85\xi/6+45\omega/2$
$7Q$					$\tau_4=7\tau_2$	$476\xi/45+84\omega/5$	$\tau_4=7\tau_2/18^*$	$35\omega/9-119\delta/18$
							$\tau_4=7\tau_2$	$119\xi/18+12\omega/2$
$5Q$			$\tau_4=5\tau_2$	$85\xi/12+45\omega/4$	$\tau_4=11\tau_2/9^*$	$20\omega/9-34\delta/9$	$\tau_4=5\tau_2/4$	$-25\xi/18-15\delta/4$
					$\tau_4=5\tau_2$	$34\xi/9+6\omega$	$\tau_4=95\tau_2/36^*$	$25\omega/18-85\delta/36$
							$\tau_4=5\tau_2$	$85\xi/36+15\omega/4$
$3Q$	$\tau_4=3\tau_2$	$34\xi/9+6\omega$	$\tau_4=3\tau_2/4$	$-5\xi/6-9\delta/4$	$\tau_4=9\tau_2/5$	$-4\xi/9-6\delta/5$	$\tau_4=9\tau_2/4$	$-5\xi/18-3\delta/4$
			$\tau_4=19\tau_2/12^*$	$5\omega/6-17\delta/12$	$\tau_4=101\tau_2/45^*$	$4\omega/9-34\delta/45$	$\tau_4=91\tau_2/36^*$	$5\omega/18-17\delta/36$
			$\tau_4=3\tau_2$	$17\xi/12+9\omega/4$	$\tau_4=3\tau_2$	$34\xi/45+6\omega/5$	$\tau_4=3\tau_2$	$17\xi/36+3\omega/4$
$1Q$	$\tau_4=\tau_2$	0	$\tau_4=\tau_2$	0	$\tau_4=\tau_2$	0	$\tau_4=\tau_2$	0
$-1Q$								
$-3Q$	$\tau_4=7\tau_2/9^*$	$-20\omega/9+34\delta/9$						
	$\tau_4=3\tau_2$	$20\xi/9+6\delta$						
$-5Q$			$\tau_4=25\tau_2/12^*$	$-25\omega/6+85\delta/12$	$\tau_4=\tau_2$	$20\xi/9+6\delta$		
			$\tau_4=25\tau_2/4$	$25\xi/6+45\delta/4$				
$-7Q$					$\tau_4=161\tau_2/45^*$	$-56\omega/9+476\delta/45$	$\tau_4=7\tau_2/2$	$35\xi/9+21\delta/2$
					$\tau_4=49\tau_2/5$	$56\xi/9+84\delta/5$		
$-9Q$							$\tau_4=31\tau_2/6^*$	$-25\omega/3+85\delta/6$
							$\tau_4=27\tau_2/2$	$25\xi/3+45\delta/2$

cycling has no effect on the $\pm 3Q\ \tau_4=3\tau_2$ echoes. Without the six-phase cycling, the $\pm 3Q\ \tau_4=3\tau_2$ echoes could be observed at the same time as the $1Q\ \tau_4=\tau_2$ echo. Since the latter has a strong amplitude, the detection threshold of the analog-digital converter of the spectrometer may prevent the detection of the $\pm 3Q\ \tau_4=3\tau_2$ echoes. On the other hand, the $-3Q\ \tau_4=7\tau_2/9$ echo has a smaller amplitude. As a result, the $\pm 3Q\ \tau_4=3\tau_2$ echoes may be observed at the same time as the $-3Q\ \tau_4=7\tau_2/9$ echo when the six-phase cycling is applied.

Table IV gathers the echo locations and the phase ϕ that modulates the maximum echo amplitudes as $\exp(-i\tau_2\phi)$ for the four half-integer quadrupole spins and the coherence order p. A pair of coherence orders $\pm p$ not equal to ± 1 generates three echoes, one of which indicated by the symbol $*$ is involved in MQ-MAS methodology. The coherence order $p=1$ always generates one echo. On the other hand, the coherence order $p=-1$, which is associated with the signal detection, does not generate echo. Therefore, 4, 7, 10, and 13 echoes are predicted for the spins $I=\frac{3}{2}$, $\frac{5}{2}$, $\frac{7}{2}$, and $\frac{9}{2}$, respectively. Among these echoes, 1, 2, 3, and 4 echoes out of 4, 7, 10, and 13, respectively, are used for MQ-MAS methodology. As mentioned in the previous paragraph, in order to observe a specific MQ echo located near the $1Q\ \tau_4=\tau_2$ one, a cycling on the phase of the first pulse and that of the receiver according to the rules of the MQ spectroscopy[37,105,106] is required.

3. Amplitudes of the Hahn echoes in the approximation of static crystal during the pulses

In Sec. III D 2 we derived the echo locations, which are determined by the interactions considered between the two pulses and during the detection period. These predictions do not depend on the spin dynamics during the pulses explicitly. Furthermore, Eqs. (68), (71), (73), and (74) show that the matrix element $\rho^{E}_{-1/2,1/2}(t_1,\tau_2,t_3,\tau_4=\lambda\tau_2)$ of the $p=-1$ central-transition echo, located at $\tau_4=\lambda\tau_2$ and describing the refocusing of the pQ on-resonance coherence generated by the first pulse, is proportional to $[\rho^{S}_{p}(t_1,t_3)]_{-1/2,1/2}$. It depends explicitly on the durations t_1 and t_3 of the two pulses. In this section we analyze the effects of these pulse durations on the echo amplitudes, which are only related to the interactions considered during the pulses and defined in Eq. (51c).

In fact Eq. (63) shows that $\rho^{E}_{-1/2,1/2}(t_1,\tau_2,t_3,\tau_4=\lambda\tau_2)$ is the product of two functions. Indeed, as the matrix form of $\rho^{S}_{p}(t_1)$ contains a single nonzero element, this latter appears as a factor in the final expression. Thus, the first function is simply the imaginary part of the single nonzero matrix element of $\rho^{S}_{p}(t_1)$. The second function or the conversion function depends only on the second-pulse duration. It is worth noting that Eqs. (54) and (63) have the same form. In the first equation, the initial state is described by $\rho(0)$, whereas in the second equation it is given by $\rho^{S}_{p}(t_1)$.

According to Eq. (49), the amplitude $E_y(t_1,\tau_2,t_3,\tau_4=\lambda\tau_2)$ of the $p=-1$ central-transition Hahn echo, located at $\tau_4=\lambda\tau_2$ and representing the refocusing of the $2rQ$ on-resonance coherence generated by the first pulse, can be defined by

$$E_y(t_1,\tau_2,t_3,\tau_4=\lambda\tau_2) = \frac{\sqrt{I(I+1)-(1/4)}}{\frac{1}{3}I(I+1)(2I+1)}\,\mathrm{Im}[\rho_{r,-r}(t_1)]\Psi^{2rQ}(t_3,\tau_4=\lambda\tau_2). \tag{75}$$

Im means the imaginary part. This definition differs slightly with our previous one,[71] in which a mistake was made because $\mathrm{Im}[\rho_{r,c}(t_1)]$ and $\langle I_y^{r,c}(t_1)\rangle$ differ by a sign.

The numerical procedure for calculating the conversion function $\Psi^{2rQ}(t_3,\tau_4=\lambda\tau_2)$ is the following: Once the matrix multiplications in Eq. (54) are performed, we generate a new matrix $\rho_{2r}^{S}(t_1)$ containing a single nonzero element $\rho_{r,-r}(t_1)$. Then we apply the matrix multiplications described by Eq. (63). We pick up the matrix element $\rho_{-1/2,1/2}^{E}(t_1,t_3)$ that we introduce in Eq. (49) to obtain the echo amplitude. Finally, the latter is divided by $\mathrm{Im}[\rho_{r,-r}(t_1)]$, yielding $\Psi^{2rQ}(t_3,\tau_4=\lambda\tau_2)$.

Figure 4 represents the graphs of the imaginary part of $3Q$, $1Q$, and $-3Q$ coherences generated by the first $-x$ pulse for a spin $I=\frac{3}{2}$ system versus the first-pulse duration t_1, for various values of $\omega_Q/(2\pi)$ and a typical pulse amplitude $\omega_{\mathrm{rf}}/(2\pi)=50$ kHz. Equation (56) shows that the $\pm3Q$ coherences have opposite signs. The imaginary part of the $3Q$ coherence is plotted versus t_1 till 60 μs to show its long pulse-duration behavior. When $\omega_Q/(2\pi)=0$ kHz, the $\pm3Q$ coherences are meaningless because they have zero amplitudes. The curve associated with $\omega_Q/(2\pi)=10$ kHz oscillates and changes sign; its extrema increase with t_1. The $\omega_Q/(2\pi)=50$ kHz curve oscillates but reaches its first maximum at about $t_1=20$ μs. The curve representing $\omega_Q/(2\pi)=200$ kHz oscillates slightly but increases steadily with t_1. The curve (not shown) associated with $\omega_Q/(2\pi)=1$ MHz is essentially zero. In the standard MAS condition, the rotating rate of a 4-mm diameter spinner reaches 10 kHz without difficulty. The approximation of a static crystal during the pulses restricts each pulse duration to 10 μs, whose inverse is 100 kHz. Thus the remaining graphs are represented for pulse durations limited to 10 μs whatever the pulse amplitude. The $\pm3Q$ coherences have large amplitudes when $\omega_Q=\omega_{\mathrm{rf}}$. Consequently, in order to have a maximum signal to noise ratio, the stronger the quadrupole coupling ω_Q and the stronger the pulse amplitude ω_{rf}. In contrast to the $\pm3Q$ coherences, the $1Q$ on-resonance coherence has large amplitudes for $\omega_Q/(2\pi)=0$ kHz and 1 MHz. These two curves are periodic with a period of 10 μs due to the choice of $\omega_{\mathrm{rf}}/(2\pi)=50$ kHz. The curves for intermediate values of ω_Q are not plotted for clarity. For short pulse duration, $1Q$ on-resonance coherence is proportional to the pulse duration t_1 and does not depend on ω_Q. This is not the case for $\pm3Q$ coherences.

Figure 5 represents the three conversion functions $\Psi^{2rQ}(t_3,\tau_4=\lambda\tau_2)$ with $r=\frac{3}{2}$, $\frac{1}{2}$, and $-\frac{3}{2}$ versus the second-pulse duration t_3 for various values of ω_Q and the same pulse amplitude $\omega_{\mathrm{rf}}/(2\pi)=50$ kHz. In contrast to the graphs of Fig. 4, these functions have the same sign independently of ω_Q and t_3. That is a property of Hahn echoes. Furthermore, alternating the phase of the second pulse without changing the receiver phase does not change the sign of the echoes.[107] The two functions $\Psi^{\pm3Q}$ are not related whereas the imaginary part of $\pm3Q$ coherences differ only by the sign. This is not surprising because Ψ^{3Q} converts the $3Q$ coherence generated by the first pulse into the $p=-1$ central-transition echo, whereas Ψ^{-3Q} converts the $-3Q$ coherence generated by the first pulse into the $p=-1$ central-transition echo. The difference between the initial and the final orders of coherence is 4 and -2 for $3Q$ and $-3Q$ coherences, respectively.

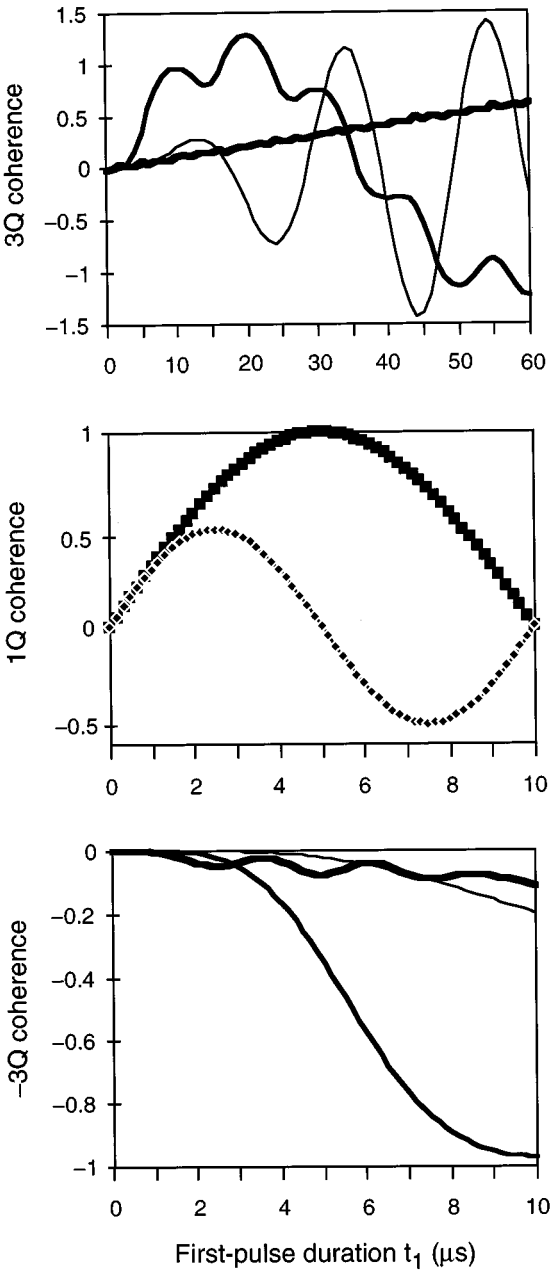

FIG. 4. Graphs of the imaginary part of the $3Q$, $1Q$, and $-3Q$ on-resonance coherences $\rho_{r,-r}(t_1)$ for a spin $I=\frac{3}{2}$ system, generated by the first pulse in a Hahn echo sequence consisting of two $-x$ pulses and in the approximation of a static crystal during the pulses, vs the first-pulse duration t_1 for $\omega_{\mathrm{rf}}/(2\pi)=50$ kHz and various values of $\omega_Q/(2\pi)$. ■: 0 kHz; thin line: 10 kHz; medium line: 50 kHz; thick line: 200 kHz; ♦: 1 MHz.

For $\omega_Q/(2\pi)=0$ kHz the three functions have large values (curves not shown for $\Psi^{\pm3Q}$). For $\omega_Q/(2\pi)=10$ kHz, Ψ^{3Q} has a large amplitude when t_3 is between 4 and 8 μs whereas Ψ^{-3Q} has a large amplitude when t_3 is between 2 and 6 μs. For $\omega_Q/(2\pi)=50$ kHz, Ψ^{3Q} reaches a peak at $t_3=5$ μs whereas Ψ^{-3Q} has a large amplitude when t_3 is between 2 and 8 μs. For $\omega_Q/(2\pi)=1$ MHz, only Ψ^{1Q} has a large amplitude, $\Psi^{\pm3Q}$ become negligible even for $\omega_Q/(2\pi)=200$ kHz. These results suggest that Ψ^{-3Q} is less affected by the

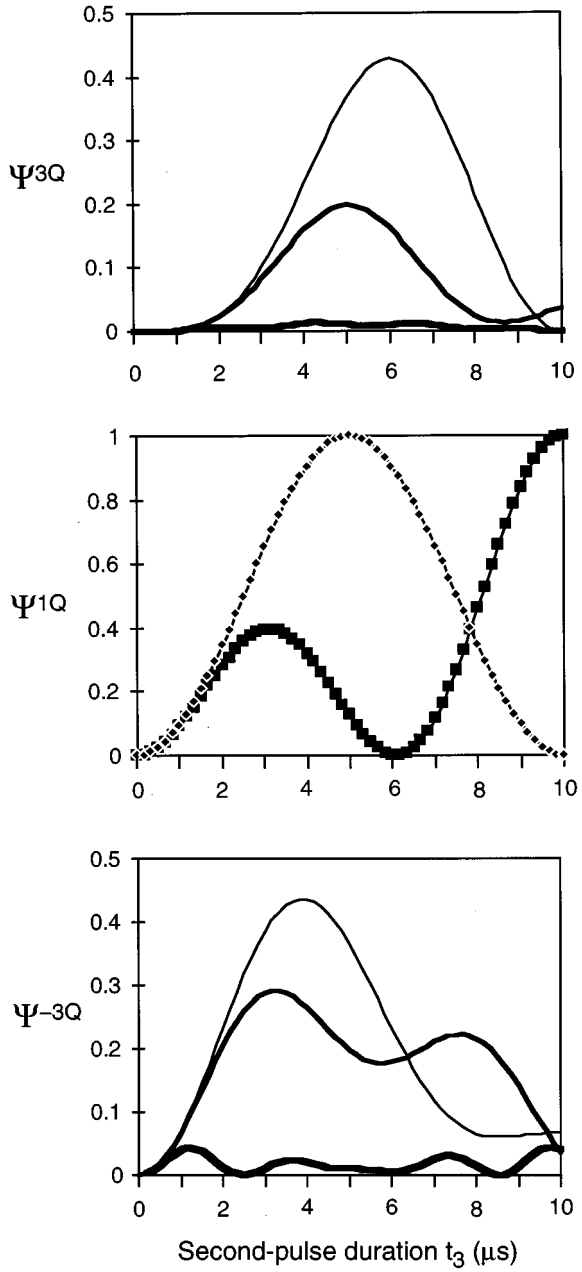

FIG. 5. Graphs of the conversion function Ψ^{2rQ} ($r=\frac{3}{2}$, $\frac{1}{2}$, and $-\frac{3}{2}$) associated with the $p=-1$ central-transition Hahn echo amplitude for a spin $I=\frac{3}{2}$ system vs the second-pulse duration t_3, for $\omega_{rf}/(2\pi)=50$ kHz and various values of $\omega_Q/(2\pi)$. The symbols and lines have the same meanings as those of Fig. 4.

second-pulse duration than Ψ^{3Q}. As in Fig. 4, Ψ^{1Q} does not depend on ω_Q for short pulse duration t_3 only. It depends on t_3 quadratically.[107]

Since a Hahn echo amplitude is the product of two functions—$\mathrm{Im}[\rho_{1/2-1/2}(t_1)]\Psi^{1Q}(t_3,\tau_4=\tau_2)$ in Eq. (75)—one depends on the first-pulse duration t_1 and the other on the second-pulse duration t_3, only the echo representing the refocusing of the $1Q$ coherence generated by the first pulse does not depends on the quadrupole coupling ω_Q if the two pulse durations are short [see Figs. 4(b) and 5(b)]. This experimental condition remains valid even for a polycrystalline sample where ω_Q presents a distribution due to the different orientations of crystallites. As a result, quantitative results on the spin population ratio may be obtained. This is not the case for the echoes of the $\pm 3Q$ coherences, whose echo amplitudes depend on ω_Q whatever the excitation condition.

III. CONCLUSIONS

First, we have derived the general expression of the MQ line shift for a half-integer quadrupole spin submitted to the first- and the second-order quadrupole interactions and located in a crystal. The latter is rotating at an arbitrary angle with respect to the magnetic field $\mathbf{B}_0$. The contribution of the first-order quadrupole interaction to the MQ line shift is suppressed either by a high spinning of the crystal at the magic angle or by the restriction to on-resonance (or symmetrical) transitions. This limits the study to the second-order quadrupole interaction only.

Then, the true isotropic chemical shift and the second-order quadrupole interaction have been considered between the two pulses and during the detection period. We have treated with great details the central-transition Hahn echoes in the simplest case of a spin $I=\frac{3}{2}$ system. Four echoes have been predicted: $1Q$ $\tau_4=\tau_2$, $\pm 3Q$ $\tau_4=3\tau_2$, and $-3Q$ $\tau_4=7\tau_2/9$ echo. In particular, the latter leads to a 2D high-resolution spectrum. For the other half-integer quadrupole spins ($I=\frac{5}{2}$, $\frac{7}{2}$, and $\frac{9}{2}$), the echo locations including those involved in MQ-MAS methodology have been defined.

Finally, applying the approximation of a static crystal and considering only the first-order quadrupole interaction during the two pulses have permitted us to analyze the echo amplitudes versus the two pulse durations. Only the $1Q$ $\tau_4=\tau_2$ echo provides us with quantitative results on the spin population ratio. In fact, our numerical approach to determining the echo amplitudes or the conversion functions can be easily extended to the other half-integer quadrupole spins.

For future work, it is desirable to remove most of the restrictions. In particular, the suppression of the approximation of a static crystal during the pulses will permit us to apply longer pulse durations. This may improve the signal to noise ratio. Rotating the crystal at the magic angle with an arbitrary spinning rate will make possible the investigation of the effects of the spinning side bandes. It is also worth including the second-order quadrupole interaction and the true isotropic chemical shift during the pulses. In that case, the reduced Wigner rotation matrix of rank four (Table II), not much applied in the present work, will be very useful.

APPENDIX

For simplicity, the following notations are used for defining the line shifts $\omega_{r,-r}=\omega_{r,-r}^{\text{fast MAS}}$ with $\omega=\omega_{-1/2,1/2}^{(2)\text{iso}}$ [Eq. (47)], $\xi=\xi_{-1/2,1/2}$ [Eq. (53a)], and $\delta=\delta_{CS}\omega_0$.

For a spin $I=\frac{5}{2}$ system,

$$\omega_{5/2,-5/2}=\tfrac{25}{4}\omega+\tfrac{25}{12}\xi-5\delta,\quad \omega_{-5/2,5/2}=-\tfrac{25}{4}\omega-\tfrac{25}{12}\xi+5\delta,$$

$$\omega_{3/2,-3/2}=-\tfrac{3}{4}\omega-\tfrac{19}{12}\xi-3\delta,\quad \omega_{-3/2,3/2}=\tfrac{3}{4}\omega+\tfrac{19}{12}\xi+3\delta,$$

$$\omega_{1/2,-1/2}=-\omega-\xi-\delta,\quad \omega_{-1/2,1/2}=\omega+\xi+\delta, \quad \text{(A1)}$$

with $\omega=-(12\Omega_Q^2/5\omega_0)(1+\frac{1}{3}\eta^2)$ and $\xi\propto 72\Omega_Q^2/\omega_0$.

For a spin $I=\frac{7}{2}$ system,

$$\omega_{7/2,-7/2}=\tfrac{49}{5}\omega+\tfrac{161}{45}\xi-7\delta,$$

$$\omega_{-7/2,7/2}=-\tfrac{49}{5}\omega-\tfrac{161}{45}\xi+7\delta,$$

$$\omega_{5/2,-5/2}=\omega-\tfrac{11}{9}\xi-5\delta,\quad \omega_{-5/2,5/2}=-\omega+\tfrac{11}{9}\xi+5\delta,$$

$$\omega_{3/2,-3/2}=-\tfrac{9}{5}\omega-\tfrac{101}{45}\xi-3\delta,\quad \omega_{-3/2,3/2}=\tfrac{9}{5}\omega+\tfrac{101}{45}\xi+3\delta,$$

$$\omega_{1/2,-1/2}=-\omega-\xi-\delta,\quad \omega_{-1/2,1/2}=\omega+\xi+\delta, \quad \text{(A2)}$$

with $\omega=-(9\Omega_Q^2/2\omega_0)(1+\frac{1}{3}\eta^2)$ and $\xi\propto 135\Omega_Q^2/\omega_0$.

For a spin $I=\frac{9}{2}$ system,

$$\omega_{9/2,-9/2}=\tfrac{27}{2}\omega+\tfrac{31}{6}\xi-9\delta,\quad \omega_{-9/2,9/2}=-\tfrac{27}{2}\omega-\tfrac{31}{6}\xi+9\delta,$$

$$\omega_{7/2,-7/2}=\tfrac{7}{2}\omega-\tfrac{7}{18}\xi-7\delta,\quad \omega_{-7/2,7/2}=-\tfrac{7}{2}\omega+\tfrac{7}{18}\xi+7\delta,$$

$$\omega_{5/2,-5/2}=-\tfrac{5}{4}\omega-\tfrac{95}{36}\xi-5\delta,\quad \omega_{-5/2,5/2}=\tfrac{5}{4}\omega+\tfrac{95}{36}\xi+5\delta,$$

$$\omega_{3/2,-3/2}=-\tfrac{9}{4}\omega-\tfrac{91}{36}\xi-3\delta,\quad \omega_{-3/2,3/2}=\tfrac{9}{4}\omega+\tfrac{91}{36}\xi+3\delta,$$

$$\omega_{1/2,-1/2}=-\omega-\xi-\delta,\quad \omega_{-1/2,1/2}=\omega+\xi+\delta, \quad \text{(A3)}$$

with $\omega=-(36\Omega_Q^2/5\omega_0)(1+\frac{1}{3}\eta^2)$ and $\xi\propto 216\Omega_Q^2/\omega_0$.

[1] A. Abragam, *Principles of Nuclear Magnetism* (Clarendon, Oxford, 1961).

[2] C. P. Slichter, *Principles of Magnetic Resonance* (Springer-Verlag, Berlin, 1990).

[3] D. Freude and J. Haase, in *NMR Basic Principles and Progress*, edited by P. Diehl, E. Fluck, H. Günter, R. Kosfeld, and J. Seelig (Springer-Verlag, Berlin, 1993), Vol. 29.

[4] M. H. Cohen and F. Reif, in *Solid State Physics*, edited by F. Seitz and D. Turnbull (Academic, New York, 1957), Vol. 5.

[5] F. Borsa and A. Rigamonti, in *Structural Phase Transitions II*, Vol. 45 of *Topics in Current Physics*, edited by K. A. Müller and H. Thomas (Springer-Verlag, Berlin, 1991).

[6] A. Rigamonti, Adv. Phys. **33**, 115 (1984).

[7] E. Lippmaa, A. Samoson, and M. Mägi, J. Am. Chem. Soc. **108**, 1730 (1986).

[8] M. T. Weller, M. E. Brenchley, D. C. Apperley, and N. A. Davies, Solid State NMR **3**, 103 (1994).

[9] P. P. Man, J. Magn. Reson. A **114**, 59 (1995).

[10] J. Skibsted, N. C. Nielsen, H. Bildsøe, and H. J. Jakobsen, J. Magn. Reson. **95**, 88 (1991).

[11] B. Herreros, P. P. Man, J.-M. Manoli, and J. Fraissard, J. Chem. Soc. Chem. Commun. 464 (1992).

[12] A. C. Kunwar, G. L. Turner, and E. Oldfield, J. Magn. Reson. **69**, 124 (1986).

[13] P. P. Man, E. Duprey, J. Fraissard, P. Tougne, and J.-B. d'Espinose, Solid State NMR **5**, 181 (1995).

[14] P. J. Chu and B. C. Gerstein, J. Chem. Phys. **91**, 2081 (1989).

[15] T. J. Bastow, J. Chem. Soc. Faraday Trans. **87**, 2453 (1991).

[16] J. Hirschinger, P. Granger, and J. Rose, J. Phys. Chem. **96**, 4815 (1992).

[17] K. Narita, J. J. Umeda, and H. Kusumoto, J. Chem. Phys. **44**, 2719 (1966).

[18] J. F. Baugher, P. C. Taylor, T. Oja, and P. J. Bray, J. Chem. Phys. **50**, 4914 (1969).

[19] A. Samoson, E. Kundla, and E. Lippmaa, J. Magn. Reson. **49**, 350 (1982).

[20] J. Skibsted, E. H. Henderson, and H. J. Jakobsen, Inorg. Chem. **32**, 1013 (1993).

[21] D. Massiot, C. Bessada, J.-P. Coutures, and F. Taulelle, J. Magn. Reson. **90**, 231 (1990).

[22] H. J. Behrens and B. Schnabel, Physica B **114**, 185 (1982).

[23] D. Müller, Ann. Phys. (Leipzig) **39**, 451 (1982).

[24] C. Fernandez, P. Bodart, and J.-P. Amoureux, Solid State NMR **3**, 79 (1994).

[25] S. Ganapathy, J. Shore, and E. Oldfield, Chem. Phys. Lett. **169**, 301 (1990).

[26] F. Lefebvre, J.-P. Amoureux, C. Fernandez, and E. G. Derouane, J. Chem. Phys. **86**, 6070 (1987).

[27] Z. Zheng, Z. Gan, N. K. Sethi, D. W. Alderman, and D. M. Grant, J. Magn. Reson. **95**, 509 (1991).

[28] A. Llor and J. Virlet, Chem. Phys. Lett. **152**, 248 (1988).

[29] P. J. Grandinetti, J. H. Baltisberger, A. Llor, Y. K. Lee, U. Werner, M. A. Eastman, and A. Pines, J. Magn. Reson. A **103**, 72 (1993).

[30] Y. Wu, B. Q. Sun, A. Pines, A. Samoson, and E. Lippmaa, J. Magn. Reson. **89**, 297 (1990).

[31] B. Q. Sun, J. H. Baltisberger, Y. Wu, A. Samoson, and A. Pines, Solid State NMR **1**, 267 (1992).

[32] B. F. Chmelka and J. W. Zwanziger, in *Solid State NMR VI: Methods and Applications of Solid-State NMR, NMR Basic Principles and Progress*, edited by B. Blümich (Springer-Verlag, Berlin, 1994), Vol. 33.

[33] A. Samoson and E. Lippmaa, J. Magn. Reson. **84**, 410 (1989).

[34] J. Butterworth, Proc. Phys. Soc. London **86**, 297 (1965).

[35] M. Mehring and O. Kanert, Z. Naturforsch. Teil A **24**, 768 (1969).

[36] O. Kanert and M. Mehring, in *NMR Basic Principles and Progress*, edited by P. Diehl, E. Fluck, and R. Kosfeld (Springer-Verlag, Berlin, 1971), Vol. 3.

[37] R. R. Ernst, G. Bodenhausen, and A. Wokaun, *Principles of Nuclear Magnetic Resonance in One and Two Dimensions* (Clarendon, Oxford, 1990).

[38] M. Goldman, *Quantum Description of High-Resolution NMR in Liquids* (Clarendon, Oxford, 1988).

[39] M. Munowitz, *Coherence and NMR* (Wiley, New York, 1988).

[40] P. P. Man, J. Magn. Reson. A **113**, 40 (1995).

[41] L. Pandey, S. Towta, and D. G. Hughes, J. Chem. Phys. **85**, 6923 (1986).

[42] L. Pandey and D. G. Hughes, J. Molec. Struct. **111**, 91 (1983).

[43] S. Ding and C. A. McDowell, J. Magn. Reson. A **112**, 36 (1995).

[44] P. P. Man, Mol. Phys. **69**, 337 (1990).

[45] S. Ding and C. A. McDowell, J. Mol. Struct. **355**, 135 (1995).

[46] P. P. Man, Mol. Phys. **78**, 307 (1993).

[47] J. A. M. van der Mijden, R. Janssen, and W. S. Veeman, Mol. Phys. **69**, 53 (1990).

[48] S. Z. Ageev and B. C. Sanctuary, Mol. Phys. **84**, 835 (1995).

[49] P. P. Man and P. Tougne, Mol. Phys. **83**, 997 (1994).

[50] P. P. Man, J. Magn. Reson. **67**, 78 (1986).

[51] P. P. Man, J. Magn. Reson. **77**, 148 (1988).

[52] D. Fenzke, D. Freude, T. Fröhlich, and J. Haase, Chem. Phys. Lett. **111**, 171 (1984).

[53] A. Samoson and E. Lippmaa, Phys. Rev. B **28**, 6567 (1983).

[54] V. H. Schmidt, in *Proceedings of the Ampere International Summer School 1971*, edited by R. Blinc (J. Stefan Institut, Ljubljana, 1972).
[55] P. P. Man, J. Klinowski, A. Trokiner, H. Zanni, and P. Papon, Chem. Phys. Lett. **151**, 143 (1988).
[56] J. Haase and E. Oldfield, J. Magn. Reson. A **104**, 1 (1993).
[57] P. P. Man, Mol. Phys. **76**, 1119 (1992).
[58] A. J. Vega, J. Magn. Reson. **96**, 50 (1992).
[59] A. J. Vega, Solid State NMR **1**, 17 (1992).
[60] P. P. Man, J. Magn. Reson. **94**, 258 (1991).
[61] P. P. Man, Solid State NMR **2**, 165 (1993).
[62] S. Vega and Y. Naor, J. Chem. Phys. **75**, 75 (1981).
[63] N. C. Nielsen, H. Bildsøe, and H. J. Jakobsen, Chem. Phys. Lett. **191**, 205 (1992).
[64] P. P. Man, Chem. Phys. Lett. **168**, 227 (1990).
[65] I. Solomon, Phys. Rev. **110**, 61 (1958).
[66] P. P. Man, Solid State NMR (to be published).
[67] P. P. Man, Z. Naturforsch. Teil A **49**, 89 (1994).
[68] N. Lee, B. C. Sanctuary, and T. K. Halstead, J. Magn. Reson. **98**, 534 (1992).
[69] T. K. Halstead, P. A. Osment, B. C. Sanctuary, J. Tegenfeldt, and I. J. Lowe, J. Magn. Reson. **67**, 267 (1986).
[70] P. P. Man, J. Chem. Phys. (to be published).
[71] P. P. Man, Phys. Rev. B **52**, 9418 (1995).
[72] E. L. Hahn, Phys. Rev. **80**, 580 (1950).
[73] D. Y. Han and H. Kessemeier, Phys. Rev. Lett. **67**, 346 (1991).
[74] P. Mansfield, Phys. Rev. A **137**, 961 (1965).
[75] J. Haase and E. Oldfield, J. Magn. Reson. A **101**, 30 (1993).
[76] L. Frydman and J. S. Harwood, J. Am. Chem. Soc. **117**, 5367 (1995).
[77] A. Medek, J. S. Harwood, and L. Frydman, J. Am. Chem. Soc. **117**, 12 779 (1995).
[78] D. Massiot, B. Touzo, D. Trumeau, J.-P. Coutures, J. Virlet, P. Florian, and P. J. Grandinetti, Solid State NMR **6**, 73 (1996).
[79] C. Fernandez, J.-P. Amoureux, L. Delmotte, and H. Kessler, Microporous Mater. **6**, 125 (1996).
[80] C. Fernandez and J.-P. Amoureux, Solid State NMR **5**, 315 (1996).
[81] G. Wu, D. Rovnyank, B. Q. Sun, and R. G. Griffin, Chem. Phys. Lett. **249**, 210 (1996).
[82] J. H. Baltisberger, Z. Xu, J. F. Stebbins, S. H. Wang, and A. Pines, J. Am. Chem. Soc. **118**, 7209 (1996).
[83] M. Mehring, *Principles of High Resolution NMR in Solids* (Springer-Verlag, Berlin, 1983).
[84] N. Chandrakumar and S. Subramanian, *Modern Techniques in High Resolution FT NMR* (Springer-Verlag, New York, 1987).
[85] G. J. Bowden and W. D. Hutchison, J. Magn. Reson. **67**, 403 (1986).
[86] R. N. Zare, *Angular Momentum* (Wiley, New York, 1988).
[87] A. Abragam and M. Goldman, *Nuclear Magnetism: Order and Disorder* (Clarendon, Oxford, 1982).
[88] H. W. Spiess, in *NMR Basic Principles and Progress*, edited by P. Diehl, E. Fluck, and R. Kosfeld (Springer-Verlag, Berlin, 1978), Vol. 15.
[89] U. Haeberlen, *High Resolution NMR in Solids, Selective Averaging* (Academic, New York, 1976).
[90] J. M. Koons, E. Hughes, H. M. Cho, and P. D. Ellis, J. Magn. Reson. A **114**, 12 (1995).
[91] M. Goldman, P. J. Grandinetti, A. Llor, Z. Olejniczak, J. R. Sachleben, and J. W. Zwanziger, J. Chem. Phys. **97**, 8947 (1992).
[92] V. Heine, *Group Theory in Quantum Mechanics* (Dover, New York, 1993).
[93] K. Takegoshi and K. Hikichi, Chem. Phys. Lett. **194**, 359 (1992).
[94] J.-P. Amoureux, Solid State NMR **2**, 83 (1993).
[95] C. Fernandez and J.-P. Amoureux, Chem. Phys. Lett. **242**, 449 (1995).
[96] S. P. Brown, S. J. Heyes, and S. Wimperis, J. Magn. Reson. A **119**, 280 (1996).
[97] A. Samoson, Chem. Phys. Lett. **247**, 203 (1995).
[98] R. Tycko and S. J. Opella, J. Chem. Phys. **86**, 1761 (1987).
[99] P. P. Man, in *Encyclopedia of Nuclear Magnetic Resonance*, edited by D. M. Grant and R. K. Harris (Wiley, Chichester, 1996).
[100] W. J. Thompson, *Angular Momentum* (Wiley, New York, 1994).
[101] D. M. Brink and G. R. Satchler, *Angular Momentum* (Clarendon, Oxford, 1968).
[102] J.-P. Amoureux, C. Fernandez, L. Carpentier, and E. Cochon, Phys. Status Solidi A **132**, 461 (1992).
[103] K. T. Mueller, B. Q. Sun, G. C. Chingas, J. W. Zwanziger, T. Terao, and A. Pines, J. Magn. Reson. **86**, 470 (1990).
[104] G. Bodenhausen, Prog. Nucl. Magn. Reson. Spectrosc. **14**, 137 (1981).
[105] J. Keeler, in *Multinuclear Magnetic Resonance in Liquids and Solids, Chemical Applications, Vol. 322 of NATO Advanced Study Institute, Series C*, edited by P. Granger and R. K. Harris (Kluwer, Dordrecht, 1990).
[106] H. Kessler, M. Gehrke, and C. Griesinger, Angew. Chem. Int. Ed. Engl. **27**, 490 (1988).
[107] P. P. Man, Appl. Magn. Reson. **4**, 65 (1993).